Pion-Nucleon Scattering and Production in the D_{13} State*

ARTHUR I. MILLER† AND EARLE L. LOMON
Laboratory for Nuclear Science and Physics Department, Massachusetts Institute of Technology, Cambridge, Massachusetts 02139
(Received 6 March 1970)

A model of the coupled πN, ρN, σN, and $\pi\Delta$ channels is adjusted to the πN scattering and pion production data below 700-MeV pion laboratory kinetic energy. A very good description is obtained of the complex D_{13} amplitude below 700 MeV, simultaneously with a good fit to the structural details of pion production in the 400–700-MeV energy interval. In computing the pion production distributions, the only addition made to the D_{13} contribution is a phase-space background accounting for 20–50% of the production cross section. The maximal interference effects between decaying resonances are investigated. Also reported are attempts to fit the data without the σN channel, but with the ωN or higher threshold channels. The cross sections for ρ, Δ, or ω production predicted at 1.0–1.5 BeV are consistent with the higher-energy data: Too much σ production is predicted.

I. INTRODUCTION

PION-NUCLEON scattering data below 1 BeV are now sufficiently detailed to have determined reasonably accurate and unambiguous complex partial-wave amplitudes.[1–3] The body of data on $\pi\pi N$ final states has also been growing[4–7] and includes enough information on momentum, mass, and angular distributions to allow an approximate analysis of the two-particle correlation and isotopic and angular momentum contents at several energies.[8] Consequently, models or theories of the pion-nucleon interaction should now be required to explain simultaneously—or at least be consistent with—the elastic scattering amplitudes and the structure of the three-body final states.

We here present a model for the D_{13} ($T=\frac{1}{2}$, $J=\frac{3}{2}$) pion-nucleon partial wave which satisfies the above requirement.

When the pion laboratory kinetic energy E_L is between 500 and 700 MeV, the resonating phase shift δ_{13} and inelasticity η_{13} are accurately described. In the same energy range, by adding a phase-space background of 20–50% to the D_{13} contribution, we obtain a good description of all observed distributions from the $\pi^-+P\rightarrow\pi+\pi+N$ reactions. Both the $\pi\pi$ and πN barycentric mass distributions are well described.

At lower energies the D_{13} contribution to the inelastic cross section becomes less than that of S and P states, and we can no longer expect the D_{13} state alone to dominate the structure of the $\pi\pi N$ distributions. The model is also not expected to give an accurate prediction for δ_{13} near elastic threshold, as it neglects the long-range character of the pion-nucleon force. In fact, the predicted value of δ_{13} falls below the experimental analysis at low energy, as would be expected from the neglect of a long-range force. The long-range character of the interaction can be added to the model without difficulty, as should be done when S- and P-wave channels are also included.

When $E_L>700$ MeV the F_{15} and D_{15} phase shifts are becoming large, rising towards resonance. Consequently, it is expected that the phase-space approximation, used in calculating the $\pi\pi N$ distributions for all but the D_{13} amplitude, will cease to be adequate. This is borne out at 646 MeV by a forward-back asymmetry in a pion angular distribution which is the only deviation from our predictions.

The chief characteristic of the model used is that it treats the coupling of the πN, ρN, σN, and $\pi\Delta$ channels nonperturbatively. There would be little value to a perturbation treatment in the resonance region. Furthermore, the ρ, σ, and Δ resonances are handled as decaying particles with their experimental mass distributions as given by a Breit-Wigner form.

The model used for the coupled-channel problem is that previously used with πN and ρN channels to explain the D_{13} resonance.[9] That was then extended to include the $\pi\Delta$ channel[10] to describe previously unexplained features of the $\pi\pi N$ states. It is a simple boundary condition model (SBCM) in which a homogeneous boundary condition is imposed on the wave function at short range, with no exterior interaction.

This is a simplification of the full boundary condition model (BCM) which includes potential-type long-range interaction. The BCM has been shown[11] to be a general representation for strong interactions with the usual analyticity and unitarity properties. It is indicated

* Work supported in part through funds provided by the Atomic Energy Commission under Contract No. AT(30-1) 2098.
† Present address: Physics Department, Lowell Technological Institute, Lowell, Mass.
[1] A. Donnachie, R. G. Kirsopp, and C. Lovelace, Phys. Letters **26B**, 161 (1968).
[2] P. Bareyre, C. Bricman, and G. Villet, Phys. Rev. **163**, 1730 (1968).
[3] C. Johnson and H. M. Steiner, LRL Report No. UCRL 18001 (unpublished).
[4] J. D. Oliver, I. Nadelhaft, and G. Yodh, Phys. Rev. **147**, 932 (1966).
[5] R. A. Burnstein *et al.*, Phys. Rev. **137**, B1044 (1965).
[6] C. N. Vittitoe *et al.*, Phys. Rev. **135**, B232 (1964).
[7] J. Kirz, J. Schwartz, and R. Tripp, Phys. Rev. **130**, 2481 (1963).
[8] D. Morgan, Phys. Rev. **166**, 1731 (1968); M. DeBeer *et al.*, Nucl. Phys. **B12**, 599 (1969).
[9] H. Goldberg and E. L. Lomon, Phys. Rev. **134**, B659 (1964).
[10] E. L. Lomon and A. I. Miller, Phys. Rev. Letters **21**, 1773 (1968).
[11] H. Feshbach and E. L. Lomon, Ann. Phys. (N. Y.) **29**, 19 (1964).

that the boundary condition matrix tends to a constant for strong interactions.

The long-range potentials are predicted by particle-exchange diagrams and are of significant strength. However, the effects being examined here (the D_{13} resonance and resonance-production thresholds) are not expected to be very sensitive to the detailed range dependence. They vary strongly with total energy rather than with momentum transfer. The long-range characteristics do matter near elastic threshold, where our model is inaccurate in its present form. The long-range behavior also determines the relative size of higher-angular-momenta partial waves. Thus to accurately describe all partial waves with a few parameters, a field-theoretical potential tail should be included.[12]

The effect of a coupled channel below its threshold is in general[13] increasingly attractive and it may readily induce a resonance.[9] Above threshold, the energy dependence of the coupled-channel contribution to the elastic amplitude decreases, and a strong inelasticity sets in. Under these conditions, the only type of resonance produced is the very inelastic type in which the phase shift does not rise through $\frac{1}{2}\pi$, but drops rapidly instead.

The strongest resonance-producing effect is expected from channels whose thresholds are closely above the resonance, and which can be produced in low-angular-momentum states. In the case of the D_{13} resonance, the natural candidates are the ρN and σN channels. The first can be produced in an S state and the other in a P state. The ω meson will affect the elastic behavior in a similar manner to the ρ meson, and will also be considered. The only other threshold in this vicinity is that of the pion paired with the $N'(1470)$, which has the same quantum numbers as the nucleon itself. It follows that the $\pi N'(1470)$ system is also in a relative D state when coupled to the πN pair in the D_{13} state. Therefore, although the threshold for $\pi N'(1470)$ is nearly 100 MeV below the ρN threshold, it is expected to have a much smaller effect in our energy region. In the three-body final-state analyses of Ref. 8, the $\pi N'(1470)$ system is determined to be present, but is much more likely to originate from the πN pair in S or P states. We do not here consider its coupling to the D_{13} state.

All lower-mass channels will strongly affect the inelasticity, but not the elastic resonance. The only low-mass channel relevant here is that of the $\pi\Delta$ system, which has long been known to be present in the final-state distributions. The $\pi\Delta$ channel is also produced in an S state. There is therefore good reason to limit the program to coupling the πN, $\pi\Delta$, ρN, σN, and ωN channels. The decays of the ρ and σ mesons play an important role in our energy region, causing dipion correlation. These correlations always peak at the upper end of the mass spectrum, as required experimentally, because of the high mass of the ρ and σ meson peaks.

We here show that the data can be adequately described without the ωN channel. It is also shown that the fit is not as good, but has many of the main features, if the σN channel is omitted but the ωN channel is included. Of course, the physical system may have important coupling among all five channels, but the absence of a one-pion-exchange diagram may make the $\pi N \rightarrow \omega N$ coupling less important than the ρ or σ production.

Previous models have failed in one or more of the following aspects: (i) They have been incorrect in the predicted behavior of the partial-wave amplitudes in this energy region[14]; (ii) they have failed to explain the dipion correlations in the several charge states[15]; (iii) they have failed to describe the πN correlations.[9,16] The model presented here is, as will be described below, good in all these respects.

In addition the model must not require unrealistic coupling strength to the isobar channels, which would predict unreasonable high-energy resonance productions. The present coupled-channel model guarantees that the experimental shape of the resonances is produced at high energy. In addition one can check the predicted magnitude of partial-wave production of resonances in the region where the resonance peak is above threshold, but where low-angular-momentum partial waves should dominate (1.3–1.5 BeV in the present case). A consistent model of the predominant low partial waves should predict a substantial part of the experimental production cross section for each resonance, but must not exceed the experimental value. The present model is also successful in this respect for the ρ, ω, and Δ production but requires some modification of the σN channel at high energies.

II. STRUCTURE OF MODEL: ELASTIC AND PRODUCTION AMPLITUDES

The general Schrödinger equation for an N-channel two-body interaction is

$$-\frac{d^2}{dr^2}\Psi+\left(U+\frac{\mathfrak{L}^2}{r^2}\right)\Psi=K^2\Psi, \qquad (1)$$

where Ψ is a column matrix of wave functions ψ_i ($i=1, \ldots, N$) for each channel and K^2 is a diagonal square matrix with diagonal components K_i^2, in which $\hbar K_i$ is the ith channel momentum determined by the total barycentric energy W and the channel masses

[12] Earle L. Lomon and Herman Feshbach, Ann. Phys. (N. Y.) 48, 94 (1968).

[13] Earle L. Lomon, Phys. Rev. D 1, 549 (1970).

[14] M. G. Olsson and G. B. Yodh, Phys. Rev. 145, 1309 (1966).

[15] R. M. Sternheimer and S. J. Lindenbaum, Phys. Rev. 109, 1723 (1958).

[16] L. F. Cook, Jr., and B. W. Lee, Phys. Rev. 127, 283 (1962); 127, 297 (1962); P. Carruthers, Ann. Phys. (N. Y.) 14, 229 (1961).

M_{iA} and M_{iB} (putting $\hbar=c=1$ in subsequent notation):

$$W=(K_i^2+M_{iA}^2)^{1/2}+(K_i^2+M_{iB}^2)^{1/2}. \quad (2)$$

$\mathfrak{L}^2$ is a diagonal matrix with diagonal components $L_i(L_i+1)$, and the interaction is represented by the $N\times N$ matrix U, whose components may be nonlocal operators. At low energies U becomes $(2M_{iR}/\hbar^2)V$, where V is the Schrödinger potential operator and the reduced mass $M_{iR}=M_{iA}M_{iB}(M_{iA}+M_{iB})^{-1}$.

Field theory indicates that at long-range U may have a simple, nearly local, representation. At short range the form of U is expected to be difficult to derive and to have the full complexity of a nonlocal energy-dependent operator. The BCM suggests[11] that the short-range effects of U can be replaced approximately by a homogeneous boundary condition at the interface r_0 between nearly local and strongly nonlocal behavior:

$$r_0\frac{d}{dr_0}\Psi=\mathfrak{f}\Psi(r_0), \quad (3)$$

where $\mathfrak{f}$ is a constant $N\times N$ matrix.

In the simplified form (the SBCM) used for this application it is assumed that $U=0$ for $r>r_0$. It follows from Eq. (1) that the components of Ψ are combinations of spherical Hankel functions. All the scattering information is now contained in Eq. (3). Specializing to the four-channel problem (and treating them as two-particle channels for the moment), the explicit form is

$$\Psi(r)=\begin{vmatrix}\psi_D(r)\\ \psi_\rho(r)\\ \psi_\Delta(r)\\ \psi_\sigma(r)\end{vmatrix}, \quad (4)$$

where $\psi_D(r)$, $\psi_\rho(r)$, $\psi_\Delta(r)$, and $\psi_\sigma(r)$ are the wave functions for $D_{13}\pi N$, $S_{13}\rho N$, $S_{13}\Delta\pi$, and $P_{13}\sigma N$ channels, respectively (all normalized to unit flux).

In the SBCM, one has

$$\psi_D(r)=(4\pi K)^{-1/2}[\phi_2^{(2)}(Kr)+S_{13}\phi_2^{(1)}(Kr)], \quad (5)$$

with $S_{13}\equiv\eta_{13}e^{2i\delta_{13}}$ and $K\equiv K_D$ for the incident channel, and

$$\psi_{\rho,\Delta}(r)=(4\pi K_{\rho,\Delta})^{-1/2}S_{\rho,\Delta}(M_{\rho,\Delta})\phi_0^{(1)}(K_{\rho,\Delta}r), \quad (6)$$

$$\psi_\sigma(r)=(4\pi K_\sigma)^{-1/2}S_\sigma(M_\sigma)\phi_1^{(1)}(K_\sigma r) \quad (7)$$

for the production channels, in which

$$\phi_L^{(m)}(Z)=Zh_L^{(m)}(Z)\quad(m=1,2), \quad (8)$$

where the $h_L^{(m)}(Z)$ are the spherical Hankel functions.[17] From Eq. (2), one has

$$K_{\rho,\sigma}=(2W)^{-1}[W^2-(M_{\rho,\sigma}+M)^2]^{1/2}\times[W^2-(M_{\rho,\sigma}-M)^2]^{1/2} \quad (9)$$

and

$$K_\Delta=(2W)^{-1}[W^2-(M_\Delta+\mu)^2]^{1/2}\times[W^2-(M_\Delta-\mu)^2]^{1/2}, \quad (10)$$

where M is the mass of the nucleon and μ is that of the pion. The S-matrix components S_i are obtained by solving Eq. (3), in which

$$\mathfrak{f}=\begin{pmatrix}f_D & f_{D\rho} & f_{D\Delta} & f_{D\sigma}\\ f_{D\rho} & f_\rho & 0 & 0\\ f_{D\Delta} & 0 & f_\Delta & 0\\ f_{D\sigma} & 0 & 0 & f_\sigma\end{pmatrix}. \quad (11)$$

Note that the resonance channels are not coupled to each other. The indirect effect of such coupling on the observables of interest is comparatively unimportant. For simplicity and to reduce parameters, such coupling is omitted here.

One may obtain ψ_ρ, ψ_Δ, and ψ_σ in terms of ψ_D from the last three linear equations represented by Eq. (3),

$$S_i=-4\pi f_{Di}[f_i+\theta_{L(i)}^+(K_iT_0)]^{-1}\times\psi_D(r_0)/\phi_{L(i)}{}^{(1)}(K_iT_0) \quad (12)$$

when $i=(\rho,\Delta,\sigma)$, and inserting this into the first linear equation, one obtains

$$r_0\,d\psi_D(r)/dr_0=f_{\rm eff}(W)\psi_D(r_0), \quad (13)$$

in which $L(i)$ is the orbital angular momentum of the channel,

$$\theta_L^+(Z)\equiv-Z\phi_L{}^{(1)\prime}(Z)/\phi_L{}^{(1)}(Z), \quad (14)$$

and

$$f_{\rm eff}(W)=f_D-\sum_{i=\rho,\Delta,\sigma}\frac{f_{Di}{}^2}{f_i+\theta_i^+(K_iT_0)}. \quad (15)$$

In our case $L(i)=(0,0,1)$, so that one needs only

$$\theta_0^+(Z)\equiv-iZ\quad\text{and}\quad\theta_1^+(Z)\equiv-iZ+i(Z+i)^{-1}. \quad (16)$$

Since the Δ, ρ, and σ particles decay, they therefore have variable masses, distributed according to the decay width Γ_i about their central mass $\bar{M}_i$ as given in Table I. This distribution is obtained from high-energy production experiments and is experimentally compatible with $|\lambda_i(M_i)|^2$, where $\lambda_i(M_i)$ is a Breit-Wigner amplitude, as expected for a resonating system. We use the relativistic Breit-Wigner forms[18]

$$\lambda_i(M_i)=\frac{N_i{}^{1/2}q_i{}^{l_i+1/2}M_i{}^{-l_i}}{(\bar{M}_i{}^2-M_i{}^2)-i\Gamma_i(\bar{M}_i{}^2/M_i)(q_i{}^*/\bar{q}_i{}^*)^{2l_i+1}}, \quad (17)$$

TABLE I. Central masses and widths of resonances and their relative angular momenta to recoil particle.

$\bar{M}_\Delta=1236$ MeV	$\Gamma_\Delta=120$ MeV	$L_\Delta=0$
$\bar{M}_\rho=765$ MeV	$\Gamma_\rho=105$ MeV	$L_\rho=0$
$\bar{M}_\sigma=720$ MeV	$\Gamma_\sigma=200$ MeV	$L_\sigma=1$
$\bar{M}_\omega=783$ MeV	$\Gamma_\omega=0$	$L_\omega=0$

[17] As defined by P. M. Morse and H. Feshbach, in *Methods of Theoretical Physics* (McGraw-Hill, New York, 1953), Pt. I.

[18] J. D. Jackson, Nuovo Cimento **34**, 1644 (1964).

where q_i^* is the momentum of either decay particle in the resonance center-of-momentum (COM) system

$$q_\Delta^* = (2M_\Delta)^{-1}[M_\Delta^2-(M+\mu)^2]^{1/2} \times[M_\Delta^2-(M-\mu)^2]^{1/2}, \quad (18)$$

$$q_{\rho,\sigma}^* = (\tfrac{1}{2}M_{\rho,\sigma}^2-\mu^2)^{1/2}, \quad (19)$$

and

$$\bar{q}_i^* \equiv q_i^*(\bar{M}_i), \quad (20)$$

and l_i is the orbital angular momentum of the decaying resonance. The normalization N_i is obtained from

$$N_i^{-1} = \int_{M_i^T}^{\infty} |\lambda_i(M_i)|^2 dM_i \quad (21)$$

integrated from threshold $M_\Delta^T = M+\mu$ and $M_{\rho,\sigma}^T = 2\mu$. The numerator of λ_i includes the quickly varying kinematic factors appropriate to the high-energy resonance-production amplitudes.[18]

This distribution of masses can be accommodated in our coupled-channel problem,[9,13] by coupling independently to the continuum of channels designated by the resonance mass: Each element of Eq. (4) becomes a continuum column matrix $\psi_i(M_i,r)$, and the off-diagonal elements of the f matrix [Eq. (11)] are replaced by the continuous distributions $\lambda_i(M_i)f_{Di}$. As before, in Eqs. (12), (13), and (15), the solution is

$$S_i(M_i) = -4\pi f_{Di}\lambda_i(M_i) \times[f_i+\theta_{L(i)}^+(K_ir_0)]^{-1}\frac{\psi_D(r_0)}{\phi_{L(i)}^{(1)}(K_ir_0)} \quad (22)$$

when $i=(\rho,\Delta,\sigma)$, and ψ_D is given by Eq. (13) with

$$f_{\rm eff}(W) = f_D - \sum_{i=\rho,\Delta,\sigma} f_{Di}^2 \int_{M_i^T}^{\infty} \frac{|\lambda_i(M_i)|^2 dM_i}{f_i+\theta_{L(i)}^+(K_ir_0)}, \quad (23)$$

with K_i now a function of M_i, as well as of W, as given by Eqs. (9) and (10).

It is important to note that for large W the kinematic dependence of Eq. (22) on M_i is dominated by $\lambda_i(M_i)$, so that the mass distribution predicted for high-energy resonance production is automatically correct.

From Eqs. (5) and (13), one easily obtains

$$S_{13} \equiv \eta_{13}e^{2i\delta_{13}} = -\left(\frac{f_{\rm eff}\phi_2^{(2)}(Z_0)-Z_0\phi_2^{(2)\prime}(Z_0)}{f_{\rm eff}\phi_2^{(1)}(Z_0)-Z_0\phi_2^{(1)\prime}(Z_0)}\right), \quad (24)$$

with $Z_0=Kr_0$, K real, from which

$$1-\eta_{13}^2 = -4\,{\rm Im}f_{\rm eff}\mathcal{S}_2[({\rm Re}f_{\rm eff}-\Delta_2)^2 + ({\rm Im}f_{\rm eff}-\mathcal{S}_2)^2]^{-1}, \quad (25)$$

where the "barrier penetration factor"

$$\mathcal{S}_2 = Z_0|\phi_2(Z_0)|^{-2} \quad (26)$$

and

$$\Delta_2 = [{\rm Re}\phi_2^{(1)}(Z_0)\,{\rm Re}\phi_2^{(1)\prime}(Z_0) - {\rm Im}\phi_2^{(1)}(Z_0)\,{\rm Im}\phi_2^{(1)\prime}(Z_0)]\mathcal{S}_2. \quad (27)$$

As Eq. (3) is unitary, one also has the relation that the total inelastic cross section

$$\sigma_{13}(W) = \frac{2\pi}{K^2}(1-\eta_{13}^2) = \frac{2\pi}{K^2}\sum_{i=\rho,\Delta,\sigma}\int_{M_i^T}^{W-m_i}|S_i(M_i,W)|^2 dM_i \equiv \sum_{i=\rho,\Delta,\sigma}\sigma_i(W), \quad (28)$$

where m_i is the mass of the third particle in the final state, $m_i=(\mu,M,M)$. It is important to note that in treating each channel independently, the unitarity relation, Eq. (28), does not include interference effects between different channels. For example, a ρN system and a $\pi\Delta$ system may decay into exactly the same $\pi\pi N$ configuration for suitably related M_ρ, M_Δ, and decay and production angles. In that case, the observed inelastic cross section will contain contributions from $S_\rho^+(M_\rho)S_\Delta(M_\Delta)$ which are not included in Eq. (28). The model is therefore not automatically unitary when interference terms are significant, a point to which we shall return later.

When $W>m_i+M_i$, there is production of the resonance and K_i is real. If $W<m_i+M_i$, then it is convenient to use the real variable

$$\chi_i \equiv -iK_i = (2W)^{-1}[(m_i+M_i)^2-W^2]^{1/2} \times[W^2-(m_i-M_i)^2]^{1/2}. \quad (29)$$

Using Eq. (16) the explicit forms of ${\rm Re}f_{\rm eff}$ and ${\rm Im}f_{\rm eff}$ [for use in Eqs. (24) and (25)] are

$$\begin{aligned}{\rm Re}f_{\rm eff}(W) = f_D &- f_\Delta f_{D\Delta}^2\int_{m+\mu}^{W-\mu}\frac{|\lambda_\Delta(M_\Delta)|^2dM_\Delta}{(K_\Delta r_0)^2+f_\Delta^2} - f_{D\Delta}^2\int_{W-\mu}^{\infty}\frac{|\lambda_\Delta(M_\Delta)|^2dM_\Delta}{\chi_\Delta r_0+f_\Delta} - f_\rho f_{D\rho}^2\int_{2\mu}^{W-M}\frac{|\lambda_\rho(M_\rho)|^2dM_\rho}{(K_\rho r_0)^2+f_\rho^2}\\ &- f_{D\rho}^2\int_{W-M}^{\infty}\frac{|\lambda_\rho(M_\rho)|^2dM_\rho}{\chi_{\rho 0}r+f_\rho} - f_{D\sigma}^2\int_{2\mu}^{W-M}\frac{[(K_\sigma r_0)^2f_\sigma+(1+f_\sigma)]|\lambda_\sigma(M_\sigma)|^2dM_\sigma}{(K_\sigma r_0)^4-(K_\sigma r_0)^2(1-f_\sigma^2)+(1+f_\sigma)^2}\\ &- f_{D\sigma}^2\int_{W-M}^{\infty}\frac{[\chi_\sigma r_0+1]|\lambda_\sigma(M_\sigma)|^2dM_\sigma}{(\chi_\sigma r_0)^2+(\chi_\sigma r_0)(1+f_\sigma)+(1+f_\sigma)} \quad (30)\end{aligned}$$

and

$$\mathrm{Im}f_{\mathrm{eff}}(W)=-f_{D\Delta}{}^2\int_{m+\mu}^{W-\mu}\frac{(K_\Delta r_0)|\lambda_\Delta(M_\Delta)|^2dM_\Delta}{(K_\Delta r_0)^2+f_\Delta{}^2}-f_{D\rho}{}^2\int_{2\mu}^{W-M}\frac{(K_\rho r_0)|\lambda_\rho(M_\rho)|^2dM_\rho}{(K_\rho r_0)^2+f_\rho{}^2}$$
$$-f_{D\sigma}{}^2\int_{2\mu}^{W-M}\frac{(K_\sigma r_0)^3|\lambda_\sigma(M_\sigma)|^2dM_\sigma}{(K_\sigma r_0)^4-(K_\sigma r_0)^2(1-f_\sigma{}^2)+(1+f_\sigma)^2}. \quad (31)$$

From Eqs. (24) and (22) we obtain the amplitudes needed to predict elastic and inelastic data. As the M_i and Γ_i are the standard values obtained from high-energy experiments, there are only eight parameters to be fitted to the lower-energy data considered here. The eight parameters are r_0, f_D, the three f_i, and the three f_{Di}, $i=(\rho,\Delta,\sigma)$.

III. THREE-BODY FINAL-STATE DISTRIBUTIONS

The above BCM amplitudes describe stable and unstable two-particle states. However, the experimental information on the detailed distribution of the decay products ($\pi\pi N$) should also be compared with the model. The model is extended to this comparison by taking into account the resonance decays. The decay amplitude has the angular distribution in the resonance COM determined by ℓ_i, the decay particle spins and the polarization of the resonance as produced. In the resonance COM the magnitude of the particle momentum is determined uniquely by the resonance mass M_i. The resonance COM coordinates are dependent on the varying resonance mass, making it necessary to convert each partial amplitude to a common coordinate system (the over-all COM system) before adding up the components. This is accomplished by inserting the proper Jacobian for each transformation.

Different resonance production amplitudes can interfere when they decay into common $\pi\pi N$ final states. We will return to the interference effect later. It is a small effect, and ambiguous. We postpone its consideration so that the dominant effect can be more clearly presented.

TABLE II. Isotopic-spin coefficients for the production and subsequent decay of the resonances.

Reaction	α_{Δ_1}	α_{Δ_2}	α_ρ	α_σ
$\pi^-+p\to\pi^-+\pi^++n$	$(2)^{-1/2}$	$(18)^{-1/2}$	$(3)^{-1/2}$	$(\frac{3}{2})^{1/2}$
$\pi^-+p\to\pi^-+\pi^0+p$	$-\frac{1}{3}$	$\frac{1}{3}$	$-(\frac{3}{2})^{1/2}$	0
$\pi^-+p\to\pi^0+\pi^0+n$	$-\frac{1}{3}$	$-\frac{1}{3}$	0	$-(3)^{-1/2}$

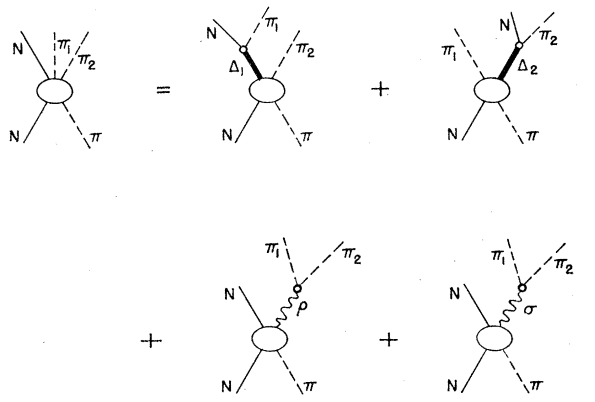

FIG. 1. Modes of resonance production included in this model.

The process $\pi N\to\pi_1\pi_2 N$ is investigated in the context of the SBCM by summing the graphs of Fig. 1. If the graphs are summed incoherently, then we have a unitary model that neglects interference. Some results for a three-channel unitary model have been given in Ref. 10. In Sec. IV the maximal interference effect will be obtained by summing the graphs of Fig. 1 coherently.

Incoherent results are presented here, in particular, the Q value (missing mass) and angular distributions in the over-all COM system for the reactions (i) $\pi^-+p\to\pi^-+\pi^++n$, (ii) $\pi^-+p\to\pi^-+\pi^0+p$, and (iii) $\pi^-+p\to\pi^0+\pi^0+n$. Charge independence is assumed in obtaining the contribution of each decaying resonance to each of the final charge states (i), (ii), and (iii). This requires only the insertion of the appropriate isospin "geometric" factors listed in Table II. The geometric factors are simple bilinear sums of Clebsch-Gordan coefficients, one Clebsch-Gordan coefficient in each product coming from the resonance formation and the other from its decay.

The fully differential form of each incoherent contribution according to the model of decaying resonances described above is first given in terms of the variables natural to the process indicated by each diagram.

(1) $\pi^-+p\to\Delta_1\pi_2\to\pi_1+N'+\pi_2$:

$$d^5\sigma_1=\tfrac{1}{2}\,\mathrm{Tr}\{(4\pi^2/K^2)\alpha_{\Delta_1}{}^2|S_{\Delta_1}(M_{\Delta_1})|^2P_{\frac{3}{2}}{}^+[\Delta_1(\Omega_1{}^{(1)}),\pi_2;S]P_{\frac{3}{2}}{}^+[\Delta_1(\Omega_1{}^{(1)}),\pi_2;S]d\Omega_1{}^{(1)}d\Omega_2dM_{\Delta_1}\}$$
$$=(\alpha_{\Delta_1}{}^2/16\pi K^2)|S_{\Delta_1}(M_{\Delta_1})|^2(1+3\cos^2\theta_1{}^{(1)})d\Omega_1{}^{(1)}d\Omega_2dM_{\Delta_1}. \quad (32)$$

(2) $\pi^-+p\to\Delta_2\pi_1\to\pi_2+N'+\pi_1$:

$$d^5\sigma_2=\tfrac{1}{2}\,\mathrm{Tr}\{(4\pi^2/K^2)\alpha_{\Delta_2}{}^2|S_{\Delta_2}(M_{\Delta_2})|^2P_{\frac{3}{2}}{}^+[\Delta_2(\Omega_2{}^{(2)})\pi_1;S]P_{\frac{3}{2}}{}^+[\Delta_2(\Omega_2{}^{(2)}),\pi_1;S]d\Omega_2{}^{(2)}d\Omega_1dM_{\Delta_2}\}$$
$$=(\alpha_{\Delta_2}{}^2/16\pi K^2)|S_{\Delta_2}(M_{\Delta_2})|^2(1+3\cos^2\theta_2{}^{(2)})d\Omega_2{}^{(2)}d\Omega_1dM_{\Delta_2}. \quad (33)$$

(3) $\pi^-+p\to\rho N'\to\pi_1+\pi_2+N'$:

$$d^5\sigma_3=\tfrac{1}{2}\,\mathrm{Tr}\{(4\pi^2/K^2)\alpha_\rho{}^2|S_\rho(M_\rho)|^2P_{\frac{3}{2}}\text{-}^+[\rho(\Omega_{1,2}{}^{(3)}),N';S]P_{\frac{3}{2}}\text{-}[\rho(\Omega_{1,2}{}^{(3)}N';S]d\Omega_{1,2}{}^{(3)}d\Omega_N dM_\rho\}$$
$$=(\alpha_\rho{}^2/16\pi K^2)|S_\rho(M_\rho)|^2(1+3\cos^2\theta_{1,2}{}^{(3)})d\Omega_{1,2}{}^{(3)}d\Omega_N dM_\rho. \quad (34)$$

(4) $\pi^-+p\to\sigma N'\to\pi_1+\pi_2+N'$:

$$d^5\sigma_4=\tfrac{1}{2}\,\mathrm{Tr}\{(4\pi^2/K^2)\alpha_\sigma{}^2|S_\sigma(M_\sigma)|^2P_{\frac{3}{2}}\text{-}^+[\sigma,N'(\Omega_N);P]P_{\frac{3}{2}}\text{-}[\sigma,N'(\Omega_N);P]d\Omega_{1,2}{}^{(4)}d\Omega_N dM\sigma\}$$
$$=(\alpha_\sigma{}^2/16\pi K^2)|S_\sigma(M_\sigma)|^2(1+3\cos^2\theta_N)d\Omega_{1,2}{}^{(4)}d\Omega_N dM_\sigma. \quad (35)$$

The solid angles of the first pion, second pion, and nucleon in the over-all COM system are Ω_1, Ω_2, and Ω_N, respectively, while in the center of mass of the resonances $i=(1,2,3,4)\to(\Delta_1,\Delta_2,\rho,\sigma)$ they are $\Omega_1{}^{(i)}$, $\Omega_2{}^{(i)}$, and $\Omega_N{}^{(i)}$, respectively. In all cases, the z axis is in the direction of the incoming beam.

The orbital and spin projection operators[19] for the production of each final state from the $D_{\frac{3}{2}}$ initial state are denoted by $P_{\frac{3}{2}}$- (resonance, third particle; relative orbital angular momentum of resonance and third particle) and their Hermitian conjugates. The ($\frac{1}{2}$ trace) operation accounts for the average over initial and sum over final nucleon spins. After the trace is taken, the resultant operator depends in each case on only one solid angle, indicated in brackets following the resonance or particle from whose distribution it arises. The other part of the system is in an S state, and its angular distribution is constant in the COM system chosen. The P_J operators are normalized by

$$\tfrac{1}{2}\,\mathrm{Tr}\int d\Omega_\alpha d\Omega_\beta d\Omega_\gamma\,(P_J{}^+P_{J'})=(J+\tfrac{1}{2})\delta_{JJ'}, \quad (36)$$

where Ω_α, Ω_β, and Ω_γ are the solid angles appropriate to the description of the three-particle final state. Table III presents the relevant projection operators.

The singly differential cross sections with respect to missing masses or the angle of one particle are obtained by integration of Eqs. (32)–(35) over the remaining variables, after transformations which separate the variable of interest.

A. Incoherent $Q(\pi N)$ Distributions

Defining the Q value in the usual way as the barycentric energy of the pair of particles less the sum of their rest masses, $Q_1\equiv Q(\pi_1 N)\equiv(M_{\Delta_1}-M-\mu)$, we obtain the following contributions to $d\sigma/dQ_1$ from each diagram.

(1) As Eq. (32) is already in terms of $dM_\Delta\equiv dQ_1$, by integration over $\Omega_1{}^{(1)}$ and Ω_2 one obtains immediately

$$\frac{d\sigma_1}{dQ_1}=\frac{2\pi}{K^2}\alpha_{\Delta_1}{}^2|S_{\Delta_1}(M_{\Delta_1})|^2. \quad (37)$$

(2) The value of Q_1 is determined by the angle between π_1 and N. In the Δ_2 COM system, N is in the opposite direction to π_2, so that Q_1 is equally well determined by $\theta_{12}{}^{(2)}$, the angle between π_1 and π_2 (in the Δ_2 COM system). The transformation in Eq. (33) of the integration variables $\Omega_2{}^{(2)}$ and Ω_1 to the integration variables $\cos\theta_1{}^{(2)}$, $\cos\theta_2{}^{(2)}$, $\cos\theta_{12}{}^{(2)}$, and $\phi_1{}^{(2)}$ is easily accomplished. As the Lorentz transformation from the over-all COM system to the Δ_2 COM system is along the π_1 direction, we have

$$d\Omega_1=d\Omega_1{}^{(2)}, \quad (38)$$

so that one need only transform from the integration variable $\phi_{21}{}^{(2)}\equiv\phi_2{}^{(1)}-\phi_1{}^{(2)}$ to $\cos\theta_{12}{}^{(2)}$. This transformation and its Jacobian are given in Appendix C in terms of over-all COM angles. One need only replace θ_2 by $\theta_2{}^{(2)}$, etc., to obtain the appropriate expressions for the present case. It follows from Eq. (33) and the above transformation that

$$\frac{d^2\sigma_2}{dM_{\Delta_2}\,d\cos\theta_{12}{}^{(2)}}=\frac{\alpha_{\Delta_2}{}^2}{16\pi K^2}|S_{\Delta_2}(M_{\Delta_2})|^2$$
$$\times\int_0^{2\pi}d\phi_1{}^{(2)}\int_{-1}^{1}d\cos\theta_2{}^{(2)}\,(1+3\cos^2\theta_2{}^{(2)})$$
$$+\int_{\cos(\theta_{12}{}^{(2)}+\theta_2{}^{(2)})}^{\cos(\theta_{12}{}^{(2)}-\theta_2{}^{(2)})}2\,d\cos\theta_1{}^{(2)}\,(\sin^2\theta_2{}^{(2)}-\cos^2\theta_1{}^{(2)}$$
$$-\cos^2\theta_{12}{}^{(2)}+2\cos\theta_1{}^{(2)}\cos\theta_2{}^{(2)}\cos\theta_{12}{}^{(2)})^{-1/2}, \quad (39)$$

where a factor 2 arises from the fact that $\theta_{12}{}^{(2)}$ goes from its minimum value $|\theta_1{}^{(2)}-\theta_2{}^{(2)}|$ to its maximum value $\theta_1{}^{(2)}+\theta_2{}^{(2)}$ and back again to its minimum, while $\phi_{12}{}^{(2)}$ goes from 0 to 2π. Equation (39) can be directly integrated to give

$$d^2\sigma_2=\alpha_{\Delta_2}{}^2(\pi/K^2)|S_{\Delta_2}(M_{\Delta_2})|^2dM_{\Delta_2}\,d\cos\theta_{12}{}^{(2)}. \quad (40)$$

With this choice of variables the integrand depends only on M_{Δ_2}. It is now convenient to transform to the over-all COM system, where the dependence on Q_1 can be expressed in terms of q_2, the momentum of π_2. Equation (40) becomes

$$d^2\sigma_2=\alpha_{\Delta_2}{}^2\frac{\pi}{K^2}|S_{\Delta_2}(M_{\Delta_2})|^2\left|\frac{dM_{\Delta_2}}{dq_2{}^{(2)}}\right|J(\mathbf{q}_2{}^{(2)}|\mathbf{q}_2)$$
$$\times\left|\frac{dq_2}{dM_{\Delta_1}}\right|dQ_1\,d\cos\theta_{12}. \quad (41)$$

[19] S. Ciulli and J. Fischer, Nuovo Cimento 12, 264 (1959).

TABLE III. Angular projection operators for initial state $J=\frac{3}{2}$, $l=2$.

Notation of Eqs. (32)–(35)	Quantum numbers of Ref. 19 l_1	j or L	l_2	Projection operators
$P_{\frac{3}{2}}{}^{-}[\Delta_1(\Omega_1{}^{(1)}),\pi_2;S]$	1	$\frac{3}{2}$	0	$(4\pi)^{-3/2}[\boldsymbol{\sigma}\cdot\hat{q}_1{}^{(1)}-3(\boldsymbol{\sigma}\cdot\hat{z})(\hat{z}\cdot\hat{q}_1{}^{(1)})]$
$P_{\frac{3}{2}}{}^{-}[\Delta_2(\Omega_2{}^{(2)}),\pi_1;S]$	1	$\frac{3}{2}$	0	$(4\pi)^{-3/2}[\boldsymbol{\sigma}\cdot\hat{q}_2{}^{(2)}-3(\boldsymbol{\sigma}\cdot\hat{z})(\hat{z}\cdot\hat{q}_2{}^{(2)})]$
$P_{\frac{3}{2}}{}^{-}[\rho(\Omega_i{}^{(3)}),N';S]$	1	1	0	$(4\pi)^{-3/2}[\boldsymbol{\sigma}\cdot\hat{q}_i{}^{(3)}-3(\boldsymbol{\sigma}\cdot\hat{z})(\hat{z}\cdot\hat{q}_i{}^{(3)})]$
$P_{\frac{3}{2}}{}^{-}[\sigma,N'(\Omega_N);P]$	0	1	1	$(4\pi)^{-3/2}[\boldsymbol{\sigma}\cdot\hat{P}-3(\boldsymbol{\sigma}\cdot\hat{z})(\hat{z}\cdot\hat{P})]$

As $q_2{}^{(2)}\equiv q_2{}^*$, the relationship of M_{Δ_2} to $q_2{}^{(1)}$ is given by Eq. (18). On the other hand, q_2 is related to M_{Δ_1} by Eq. (10); remember that $q_2=K_{\Delta_1}$. The momentum and angular transformations are given in Appendix A. The above Jacobian J of the Lorentz transformation depends only on $q_2{}^{(2)}$ and $\cos\theta_{12}{}^{(2)}$ and is given in Appendix B. By numerical integration of Eq. (41) with respect to $\cos\theta_{12}$,

$$\frac{d\sigma_2}{dQ_1}=\int\frac{d^2\sigma_2}{dQ_1\,d\cos\theta_{12}}d\cos\theta_{12}, \tag{42}$$

one obtains the contribution of process (2) to the Q_1 distribution.

(3) The angular dependence of Eq. (34) can be obtained from that of Eq. (33) by substitution of $\Omega_2{}^{(3)}$ for $\Omega_2{}^{(2)}$ and of Ω_N for Ω_1. It follows that by Lorentz transforming Ω_N to $\Omega_N{}^{(3)}$ and changing to the variable $\cos\theta_{2N}{}^{(3)}$ from $\phi_N{}^{(3)}$, one obtains a result analagous to Eq. (39). Then by integration over $\phi_2{}^{(3)}$, $\cos\theta_2{}^{(3)}$, and $\cos\theta_N{}^{(3)}$, one obtains the analog of Eq. (40):

$$d^2\sigma_3=\alpha_\rho{}^2(\pi/K^2)\,|S_\rho(M_\rho)|^2dM_\rho d\cos\theta_{2N}{}^{(3)}, \tag{43}$$

whose integrand is independent of $\cos\theta_{2N}{}^{(3)}$. By transforming into the over-all COM system, one can again take advantage of the relationship between M_{Δ_1} and q_2:

$$d^2\sigma_3=\alpha_\rho{}^2\frac{\pi}{k^2}|S_\rho(M_\rho)|^2\left|\frac{dM_\rho}{dq_2{}^{(3)}}\right|J(\mathbf{q}_2{}^{(3)}|\mathbf{q}_2)\times\left|\frac{dq_2}{dM_{\Delta_1}}\right|dQ_1\,d\cos\theta_{2N}, \tag{44}$$

where M_ρ is related to $q_2{}^{(3)}\equiv q_2{}^*$ by Eq. (19), and the new Jacobian J depends only on $q_2{}^{(3)}$ and $\cos\theta_{2N}{}^{(3)}$ and is given in Appendix B. In this case one integrates Eq. (44) to obtain

$$\frac{d\sigma_3}{dQ_1}=\int\frac{d^2\sigma_3}{dQ_1\,d\cos\theta_{2N}}d\cos\theta_{2N}. \tag{45}$$

(4) In making a Lorentz transformation from Ω_N to $\Omega_N{}^{(4)}$, the frame velocity is in the direction of the nucleon, so that $\Omega_N{}^{(4)}=\Omega_N$, as well as $d\Omega_N{}^{(4)}=d\Omega_N$. One can then follow the analog of the procedure used to obtain Eq. (43), i.e., change to the variable $\cos\theta_{2N}{}^{(4)}$ from $\phi_N{}^{(4)}-\phi_2{}^{(4)}$ and integrate over $\phi_2{}^{(4)}$, $\cos\theta_2{}^{(4)}$, and $\cos\theta_N{}^{(4)}$, obtaining

$$d^2\sigma_4=\alpha_\sigma{}^2(\pi/K^2)\,|S_\sigma(M_\sigma)|^2dM_\sigma\,d\cos\theta_{2N}{}^{(4)}. \tag{46}$$

As Eq. (46) can be obtained from Eq. (43) by replacing the subscript ρ with σ and the superscript (3) with (4), we can immediately obtain the analog of Eqs. (44) and (45) by the same replacements.

The value of $d\sigma/dQ_1$ is now obtained by the addition of $d\sigma_i/dQ_1$ for $i=(1,2,3,4)$. The integrations are considerably simplified by the absence of angular dependence in the intermediate Eqs. (40) and (43) and the σ analog, Eq. (43). This simplicity has come about in spite of the production polarization of the Δ and ρ, and the P-wave production distribution of the σ resonance.

$d\sigma/dQ_2$ is obtained by interchange of the subscripts 1 and 2 in the above formulas. This amounts to the interchange of $\alpha_{\Delta_1}{}^2$ with $\alpha_{\Delta_2}{}^2$.

B. Incoherent $Q(\pi_1\pi_2)$ Distributions

For $Q_{\pi\pi}\equiv(M_{\rho,\sigma}-2\mu)$, the contributions of processes (1) and (2) to $d\sigma/dQ_{\pi\pi}$ differ only by $\alpha_{\Delta_i}{}^2$. In either case the value of $Q_{\pi\pi}$ is determined by $\cos\theta_{12}{}^{(i)}$ so that it is convenient to make the transformations and integrations that lead from Eqs. (33) to (40). Following that, one must transform from the integration variable M_{Δ_i} to the nucleon momentum P, rather than to q_2, as P determines M_ρ or M_σ. Making the appropriate transformations, one obtains, from Eq. (40),

$$\frac{d\sigma_1}{dQ_{\pi\pi}}=\frac{\pi}{K^2}\alpha_{\Delta_1}{}^2|S_{\Delta_1}(M_{\Delta_1})|^2\left|\frac{dM_{\Delta_1}}{dP^{(1)}}\right|J(\mathbf{P}^{(1)}|\mathbf{P})\times\left|\frac{dP}{dM_{\pi\pi}}\right|d\cos\theta_{2N}, \tag{47}$$

while $d\sigma_2/dQ_{\pi\pi}$ is obtained by the interchange of indices 1 and 2. The momentum and angular transformations are given in Appendix A, the required kinematic relations are in Eqs. (9) and (18), and the Jacobian is in Appendix B.

As M_ρ and M_σ are equivalent to $M_{\pi\pi}$, the contributions of processes (3) and (4) are obtained by integration of Eqs. (34) and (35) over all variables other than M_ρ or M_σ:

$$\frac{d\sigma_{3,4}}{dQ_{\pi\pi}}=\frac{2\pi}{K^2}\alpha_{\rho,\sigma}{}^2|S_{\rho,\sigma}(M_{\rho,\sigma})|^2. \tag{48}$$

Addition of the four contributions of Eqs. (47) and (48) gives $d\sigma/dQ_{\pi\pi}$.

C. Incoherent Angular Distributions

The pion angular distribution in the over-all COM system contributed by each of the four processes is obtained from Eqs. (32)–(35). The first process yields an isotropic distribution in θ_2. Recognizing that $S_{\Delta_1}(M_{\Delta_1})$ is independent of $\Omega_1^{(1)}$, the integration over $\Omega_1^{(1)}$ and ϕ_2 in Eq. (32) is easily performed to give

$$\frac{d\sigma_1}{d\cos\theta_2}=\alpha_{\Delta_1}{}^2\frac{\pi}{K^2}\int|S_{\Delta_1}(M_{\Delta_1})|^2dM_{\Delta_1}. \tag{49}$$

For processes (2)–(4), Eqs. (33)–(35) are manipulated similarly. In the expression for $d^5\sigma_i$ $(i=2,3,4)$ the transformation $dM_i\rightarrow|dM_i/dq_2{}^{(i)}|dq_2{}^{(i)}$ is followed by the transformation $dq_2{}^{(i)}d\Omega_2{}^{(i)}\rightarrow J(\mathbf{q}_2{}^{(i)}|\mathbf{q}_2)\times dq_2d\Omega_2$. The momentum and angular transformations are listed in Appendix A, and the Jacobians J in Appendix B. Integration over $d\Omega_1$ for process (2), $d\Omega_N$ for processes (3) and (4), and over q_2 and ϕ_2 (there is no ϕ_2 dependence) for all three cases yields $d\sigma_i/d\cos\theta_2$. We collect these results together with that of Eq. (49):

$$\begin{aligned}\frac{d\sigma}{d\cos\theta_2}=&\alpha_{\Delta_1}{}^2\frac{\pi}{K^2}\int|S_{\Delta_1}(M_{\Delta_1})|^2dM_{\Delta_1}+\frac{\alpha_{\Delta_2}{}^2}{8K^2}\int\int|S_{\Delta_2}(M_{\Delta_2})|^2\left|\frac{dM_{\Delta_2}}{dq_2{}^{(2)}}\right|J(\mathbf{q}_2{}^{(2)},|\mathbf{q}_2)(1+3\cos^2\theta_2{}^{(2)})dq_2d\Omega_1\\&+\frac{\alpha_\rho{}^2}{8K^2}\int\int|S_\rho(M_\rho)|^2\left|\frac{dM_\rho}{dq_2{}^{(3)}}\right|J(\mathbf{q}_2{}^{(3)}|\mathbf{q}_2)(1+3\cos^2\theta_2{}^{(3)})dq_2d\Omega_N\\&+\frac{\alpha_\sigma{}^2}{8K^2}\int\int|S_\sigma(M_\sigma)|^2\left|\frac{dM_\sigma}{dq_2{}^{(4)}}\right|J(\mathbf{q}_2{}^{(4)}|\mathbf{q}_2)(1+3\cos^2\theta_N)dq_2d\Omega_N.\end{aligned} \tag{50}$$

The equation for the nucleon angular distribution in the over-all COM system is derived by the same procedures as the one for $d\sigma/d\Omega_2$, and we shall only write the result:

$$\begin{aligned}\frac{d\sigma}{d\cos\theta_N}=&\frac{\pi}{K^2}\alpha_\rho{}^2\int|S_\rho(M_\rho)|^2dM_\rho+\frac{\pi}{2K^2}\alpha_\sigma{}^2(1+3\cos^2\theta_N)\int|S_\sigma(M_\sigma)|^2dM_\sigma\\&+\frac{(\alpha_{\Delta_1}{}^2+\alpha_{\Delta_2}{}^2)}{8K^2}\int\int|S_{\Delta_2}(M_{\Delta_2})|^2\left|\frac{dM_{\Delta_2}}{dP^{(2)}}\right|(1+3\cos^2\theta_N{}^{(2)})J(\mathbf{P}^{(2)}|\mathbf{P})dPd\Omega_1.\end{aligned} \tag{51}$$

IV. INTERFERENCE OF DECAY PROCESSES

Interference effects are obtained in adding the amplitudes, rather than the cross sections, of each of the four production processes for the same three-body kinematic variables. These amplitudes are given *at the position of decay* by the initial expressions of Eqs. (32)–(35), in which the modulus and trace operations are only formally indicated. Insofar as the resonances are produced over a finite range and propagate a finite distance before decay, extra phase factors are introduced that are not included in our formalism. The appropriate average over the space-time displacements would, because of the oscillating phase, decrease the interference terms. By ignoring this additional phase, one obtains an upper limit on the interference effects, bounded by the given production phase and, most importantly, the experimentally known Breit-Wigner resonance phase of the decaying particles. We are content with this upper limit for the present as we find the interference effects to be small. Previous calculations of interference effects made the same approximation although large interference terms were predicted.[14]

The amplitudes as expressed in Eqs. (32)–(35) are each appropriate to a different phase space. To compute the interference of a pair of processes each of the pair of amplitudes must first we transformed to a common phase space. One dimension of this space must be the variable with respect to which the differential cross section is derived; in this case $dM_{\Delta_1}\equiv dQ_1$. The other four independent variables may be chosen at will for each pair of amplitudes. The choice is discussed below.

The Jacobian of the necessary transformation of the variables of the ith process when paired with the jth process $(i,j=1,\ldots,4)$ is denoted as $J_i(ij)$. From Eqs. (32)–(35), one then has

$$A_i(ij)=(2\pi/K)\alpha_iS_i(M_i)P_{\frac{i}{2}}(i)[J_i(ij)]^{1/2}. \tag{52}$$

The contribution to the cross section of the interference between the ith and jth process is then given by

$$\frac{d\sigma_{ij}}{dQ_1}=\int d^4\gamma_{ij}\,\mathrm{Tr}[\mathrm{Re}A_i{}^\dagger(ij)A_j(ji)], \tag{53}$$

where γ_{ij} is the chosen set of four independent variables.

The trace operation is relevant only to the products of the projection operators. As previously noted, each of these operators depends on only one direction which

we now label with a unit vector $\hat{t}^i$ such that

$$\hat{t}^1=\hat{q}_1^{(1)} \quad \text{or} \quad \hat{P}^{(1)}, \quad \hat{t}^2=\hat{q}_2^{(2)} \quad \text{or} \quad \hat{P}^{(2)},$$

$$\hat{t}^3=\hat{q}_1^{(3)} \quad \text{or} \quad \hat{q}_2^{(3)}, \tag{54}$$

and

$$\hat{t}^4=\hat{P}.$$

As a result,

$$\tfrac{1}{2}\,\mathrm{Tr}P_{\frac{3}{2}}{}^{-+}(i)P_{\frac{3}{2}}{}^{-}(j) = (64\pi^3)^{-1}[\hat{t}^i\cdot\hat{t}^j+3(\hat{t}^i\cdot\hat{z})(\hat{t}^j\cdot\hat{z})], \tag{55}$$

where $\hat{z}$ is a unit vector in the beam direction.

In each case one can choose $\hat{t}^j$ $(j=1, 2, 3)$ such that the direction of Lorentz transformation to the over-all COM system from the indicated resonance COM system is the direction of $\hat{t}^i$. For instance, in considering $\hat{t}^1\cdot\hat{t}^2$ the choice is $\hat{q}_1^{(1)}$ and $\hat{q}_2^{(2)}$, for $\hat{t}^1\cdot\hat{t}^3$ it is $\hat{P}^{(1)}$ and $\hat{q}_1^{(3)}$, and for $\hat{t}^1\cdot\hat{t}^4$ it is $\hat{P}^{(1)}$ and $\hat{P}$. It follows that $\hat{t}^1\cdot\hat{t}^2$ depends only on $\hat{q}_1\cdot\hat{q}_2$ and therefore only on θ_{12}, the angle between the pions in the over-all COM system; $\hat{t}^1\cdot\hat{t}^3$ depends only on θ_{1N}, the angle between the first pion and the nucleon in the over-all COM system, and so on for each pair, the full relations being given in Appendix C. The $J_i(ij)$ discussed below have, apart from the transformation from azimuthal to relative angles given explicitly in Appendix C, an angular dependence arising from the above Lorentz transformations depending on the same relative angles.

The dependence of the interference term between the first two processes on $\cos\theta_1$ and $\cos\theta_2$ is entirely in the term $(\hat{t}^1\cdot\hat{z})(\hat{t}^2\cdot\hat{z})$. The integration over $\cos\theta_1$ and $\cos\theta_2$ is easily performed, as in Appendix C, leaving only a $\cos\theta_{12}$ dependence [$(\phi_2-\phi_1)$ has been replaced by the $\cos\theta_{12}$ dependence]. There is no dependence on ϕ_1 so that the ϕ_1 integration is trivial. A similar reduction to an integral over the relative angle in the over-all COM system is possible for each pair. The four-dimensional integral of Eq. (53) is easily reduced to a one-dimensional integral.

An example will illustrate the formulation of $J_i(ij)$. Consider $d\sigma_{23}/dQ_1$, in which the integrations can be reduced to a numerical integral over $\cos\theta_{1N}$, where θ_{1N} is the relative angle between the first pion and the outgoing nucleon in the over-all COM system. The steps which lead to the integration variables $\cos\theta_1$, $\cos\theta_N$, ϕ_N, $\cos\theta_{1N}$, and M_{Δ_1} are as follows: The phase space for A_2 [Eq. (33)] is (noting the equivalence of $\Omega_2^{(2)}$ and $\Omega_N^{(2)}$)

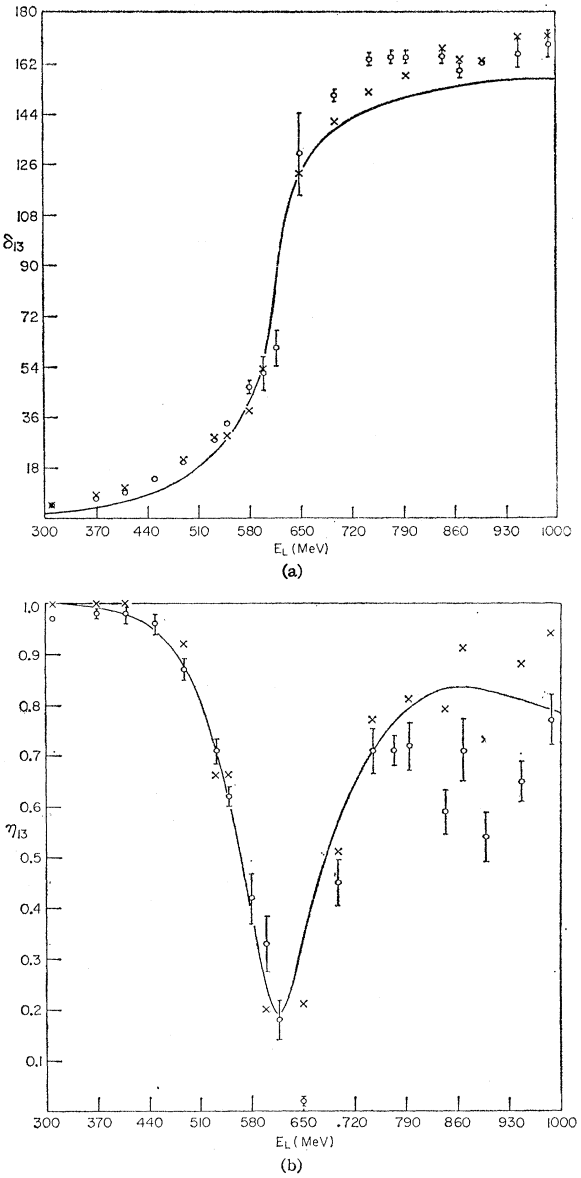

FIG. 2. $\rho\Delta\sigma$ model fit to (a) δ_{13} and (b) η_{13}. The data points designated by O are from Ref. 1, and those represented by × are from Ref. 3. The model parameters are $f_D=5.55$, $f_\rho=0.40$, $f_\Delta=2.80$, $f_\sigma=0.0$, $f_{D\rho}=2.47$, $f_{D\Delta}=2.40$, and $f_{D\sigma}=7.0$.

$$\begin{aligned}
d\Omega_N^{(2)}d\Omega_1 dM_{\Delta_2} &\to |dM_{\Delta_2}/dP^{(2)}|\,d^3P^{(2)}d\Omega_1\\
&\to |dM_{\Delta_2}/dP^{(2)}|\,J(\mathbf{P}^{(2)}|\mathbf{P})d^3Pd\Omega_1\\
&\to |dM_{\Delta_2}/dP^{(2)}|\,J(\mathbf{P}^{(2)}|\mathbf{P})J(\phi_N,\phi_1|\ \cos\theta_{1N},\phi_N)dP\ d\cos\theta_N\ d\cos\theta_1\ d\cos\theta_{1N}\ d\phi_N\\
&\to |dM_{\Delta_2}/dP^{(2)}|\,J(\mathbf{P}^{(2)}|\mathbf{P})J(\phi_N,\phi_1|\ \cos\theta_{1N},\phi_N)|\,\partial P/\partial q_2|_{\cos\theta_{1N}}\\
&\quad\times|dq_2/dM_{\Delta_1}|\,d\cos\theta_N\ d\cos\theta_1\ d\cos\theta_{1N}\ d\phi_N dQ_1\\
&\equiv J_2(23)\ d\cos\theta_N\ d\cos\theta_1\ d\cos\theta_{1N}\ d\phi_N dQ_1,
\end{aligned} \tag{56}$$

and the phase space for A_3 [Eq. (34)] is

$$\begin{aligned}
d\Omega_1^{(3)}d\Omega_N dM_\rho &\to |dM_\rho/dq_1^{(3)}|\, d^3q_1^{(3)}d\Omega_N \\
&\to |dM_\rho/dq_1^{(3)}|\, J(\mathbf{q}_1^{(3)}|\mathbf{q}_1) d^3q_1 d\Omega_N \\
&\to |dM_\rho/dq_1^{(3)}|\, J(\mathbf{q}_1^{(3)}|\mathbf{q}_1) J(\phi_N,\phi_1|\cos\theta_{1N},\phi_N) dq_1\, d\cos\theta_N\, d\cos\theta_1\, d\cos\theta_{1N}\, d\phi_N \\
&\to |dM_\rho/dq_1^{(3)}|\, J(\mathbf{q}_1^{(3)}|\mathbf{q}_1) J(\phi_N,\phi_1|\ \cos\theta_{1N},\phi_N)|\, \partial q_1/\partial q_2|_{\cos\theta_{1N}} \\
&\quad \times |dq_2/dM_{\Delta_1}|\ d\cos\theta_N\, d\cos\theta_1\, d\cos\theta_{1N}\, d\phi_N dQ_1 \\
&\equiv J_3(23)\ d\cos\theta_N\, d\cos\theta_1\, d\cos\theta_{1N}\, d\phi_N dQ_1. \qquad (57)
\end{aligned}$$

The other $J_i(ij)$ are evolved in a similar way. The result is that

$$\begin{aligned}
\frac{K^2}{2\pi}\frac{d\sigma_{\rm int}}{dQ_1} &= \alpha_{\Delta_1}\alpha_{\Delta_2}\int d\cos\theta_{12}\ \mathrm{Re}[S_{\Delta_1}{}^*(M_{\Delta_1})S_{\Delta_2}(M_{\Delta_2})]\hat{q}_1{}^{(1)}\cdot\hat{q}_2{}^{(2)} \\
&\times\left|\frac{dq_2}{dM_{\Delta_1}}\right|\left[\left|\frac{dM_{\Delta_1}}{dq_1{}^{(1)}}\frac{dM_{\Delta_2}}{dq_2{}^{(2)}}\left(\frac{\partial q_1}{\partial q_2}\right)_{\theta_{12}}\right| J(\mathbf{q}_1{}^{(1)}|\mathbf{q}_1)J(\mathbf{q}_2{}^{(2)}|\mathbf{q}_2)\right]^{1/2} \\
&+\alpha_{\Delta_1}\int d\cos\theta_{2N}\ \mathrm{Re}\{S_{\Delta_1}{}^*(M_{\Delta_1})[\alpha_\rho S_\rho(M_3)\hat{P}^{(1)}\cdot\hat{q}_2{}^{(3)}+\alpha_\sigma S_\sigma(M_3)\hat{P}^{(1)}\cdot\hat{P}]\}\left[\left|\frac{dq_2}{dM_{\Delta_1}}\frac{dM_3}{dq_2{}^{(3)}}\right| J(\mathbf{q}_2{}^{(3)}|\mathbf{q}_2)\right]^{1/2} \\
&+\alpha_{\Delta_2}\int d\cos\theta_{1N}\ \mathrm{Re}\{S_{\Delta_2}{}^*(M_{\Delta_2})[\alpha_\rho S_\rho(M_3)\hat{P}^{(2)}\cdot\hat{q}_1{}^{(3)}+\alpha_\sigma S_\sigma(M_3)\hat{P}^{(2)}\cdot\hat{P}]\} \\
&\times\left|\frac{dq_2}{dM_{\Delta_1}}\right|\left[\left|\frac{dM_{\Delta_2}}{dP^{(2)}}\frac{dM_3}{dq_1{}^{(3)}}\left(\frac{\partial P}{\partial q_2}\right)_{\theta_{1N}}\left(\frac{\partial q_1}{\partial q_2}\right)_{\theta_{1N}}\right| J(\mathbf{P}^{(2)}|\mathbf{P})J(\mathbf{q}_1{}^{(3)}|\mathbf{q}_1)\right]^{1/2} \\
&+\alpha_\rho\alpha_\sigma\int d\cos\theta_{2N}\ \mathrm{Re}[S_\rho{}^*(M_3)S_\sigma(M_3)]\hat{P}\cdot\hat{q}_2{}^{(3)}\left|\frac{dM_3}{dq_2{}^{(3)}}\frac{dq_2}{dM_{\Delta_1}}\right| J(\mathbf{q}_2{}^{(3)}|\mathbf{q}_2). \qquad (58)
\end{aligned}$$

In the above, M_3 replaces the common kinematical values of M_ρ and M_σ.

The expression for $d\sigma_{\rm int}/dQ_2$ is obtained by interchanging the coordinates for the first and second pion. This means in effect the interchange of the Clebsch-Gordon coefficients.

To obtain $d\sigma_{\rm int}/dQ_{\pi\pi}$, the chains of transformations (56) and (57) are altered so that $dQ_{\pi\pi}$ replaces dQ_1, which requires that $dP \to |dP/dM_3|\, dQ_{\pi\pi}$ while $dq_{1,2} \to |(\partial q_{1,2}/\partial P)dP/dM_3|\, dQ_{\pi\pi}$, where the appropriate angle is held constant in the partial derivative. The result is

$$\begin{aligned}
\frac{K^2}{2\pi}\frac{d\sigma_{\rm int}}{dQ_{\pi\pi}} &= \alpha_{\Delta_1}\alpha_{\Delta_2}\int d\cos\theta_{12}\ \mathrm{Re}[S_{\Delta_1}{}^*(M_{\Delta_1})S_{\Delta_2}(M_{\Delta_2})]\hat{q}_1{}^{(1)}\cdot\hat{q}_2{}^{(2)} \\
&\times\left|\frac{dP}{dM_3}\right|\left[\left|\frac{dM_{\Delta_1}}{dq_1{}^{(1)}}\frac{dM_{\Delta_2}}{dq_2{}^{(2)}}\left(\frac{\partial q_1}{\partial P}\right)_{\theta_{12}}\left(\frac{\partial q_2}{\partial P}\right)_{\theta_{12}}\right| J(\mathbf{q}_1{}^{(1)}|\mathbf{q}_1)J(\mathbf{q}_2{}^{(2)}|\mathbf{q}_2)\right]^{1/2} \\
&+\alpha_{\Delta_1}\int d\cos\theta_{2N}\ \mathrm{Re}\{S_{\Delta_1}{}^*(M_{\Delta_1})[\alpha_\rho S_\rho(M_3)\hat{P}^{(1)}\cdot\hat{q}_2{}^{(3)}+\alpha_\sigma S_\sigma(M_3)\hat{P}^{(1)}\cdot\hat{P}]\} \\
&\times\left|\left(\frac{\partial q_2}{\partial P}\right)_{\theta_{2N}}\frac{dP}{dM_3}\right|\left[\left|\frac{dM_{\Delta_1}}{dq_2}\right| J(\mathbf{q}_2{}^{(3)}|\mathbf{q}_2)\right]^{1/2} \\
&+\alpha_{\Delta_2}\int d\cos\theta_{1N}\ \mathrm{Re}\{S_{\Delta_2}{}^*(M_{\Delta_2})[\alpha_\rho S_\rho(M_3)\hat{P}^{(2)}\cdot\hat{q}_1{}^{(3)}+\alpha_\sigma S_\sigma(M_3)\times\hat{P}^{(2)}\cdot\hat{P}]\} \\
&\times\left|\left(\frac{\partial q_1}{\partial P}\right)_{\theta_{2N}}\frac{dP}{dM_3}\right|\left[\left|\frac{dM_{\Delta_2}}{dq_1}\right| J(\mathbf{q}_1{}^{(3)}|\mathbf{q}_1)\right]^{1/2}. \qquad (59)
\end{aligned}$$

The ρ-σ interference term vanishes, because of its orthogonal angular dependence. The equivalent to the last term of Eq. (58) lacks the factor

$$|(dM_3/dq_2{}^{(3)})(dq_2/dM_{\Delta_1})|\,.$$

The inverse Lorentz transformation $J(\mathbf{q}_2|q_2{}^{(3)})$ may be performed, leading to

$$\int_{-1}^{1} d\cos\theta_{2N}{}^{(3)}\,\hat{P}\cdot\hat{q}_2{}^{(3)}=0.$$

Equations (58) (and the trivial change for the Q_2 dependence) and (59) contain the results of this section. When calculated for the model S_i, they yield upper limits for interference effects. The spatial distribution of the decays will decrease the physical interference effects.

We have not given the expressions for the resonance interference effects in angular distributions. We expect them to be small, and the angular distribution data do not have sufficient accuracy to test small effects. The interference effects between partial waves will be much more important in fitting angular distribution data, and we are not able to examine those until the other partial waves are treated in such detail as the present D_{13}-channel calculation.

V. DATA FIT AND PREDICTIONS

The choice of coupled channels has been discussed in the Introduction. In particular there is a need for channels with higher thresholds than the obviously important $\pi\Delta$ system to produce the D_{13} resonance. Furthermore, the high-mass peaking in the $\pi^+\pi^-$ and the $\pi^-\pi^0$ barycentric mass distributions indicates the contribution of at least one boson with $T>0$ that decays into two pions. This requires the ρN channel, as the only appropriate system in the correct mass range, to be coupled.

This minimal three-channel (πN,ρN,$\pi\Delta$) system was fitted to the data in Ref. 10. The complex D_{13} amplitude was accurately predicted, and the qualitative features of the πN and $\pi\pi$ barycentric mass distributions in the three-body final state were qualitatively explained. However, the dipion mass peaking was much too pronounced, and too much branching to the $\pi^-\pi^0 p$ channel was predicted. In addition, the πN barycentric mass distribution was insufficiently sharply peaked, indicating that the proportion of the $\pi\Delta$ channel was too small.

The deficiencies of the above three-channel model are most easily removed by the additional coupling to a σN channel, if the σ meson is a $T=0$, $J^P=0^+$ dipion, with about the ρ mass, decaying strongly into two mesons. Recent evidence [20,21] corroborates the existence of such a meson, with a very large width, with the parameters

[20] E. Malamud and P. E. Schlein, Phys. Rev. Letters **19**, 1056 (1967).

[21] M. Feldman *et al.*, Phys. Rev. Letters **22**, 316 (1969); G. A. Smith and R. J. Manning, Phys. Rev. **171**, 1399 (1968).

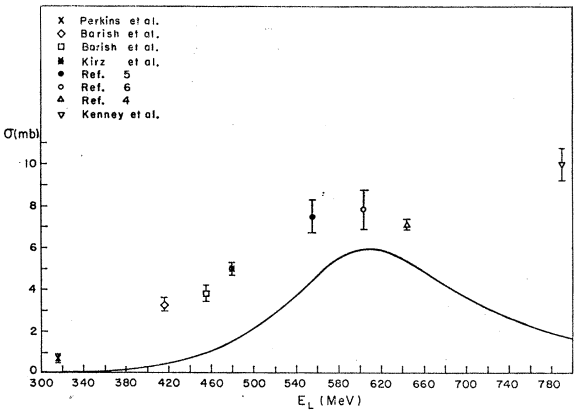

FIG. 3. Cross section generated by the $\rho\Delta\sigma$ model for $\pi^-+p\to\pi^-+\pi^++n$ from the initial D_{13} state. The references are W. Perkins *et al.*, Phys. Rev. **118**, 1364 (1960); B. Barish *et al.*, *ibid.* **135**, B416 (1964); J. Kirz *et al.*, *ibid.* **130**, 2481 (1963); and V. Kenney *et al.*, Bull. Am. Phys. Soc. **8**, 523 (1963).

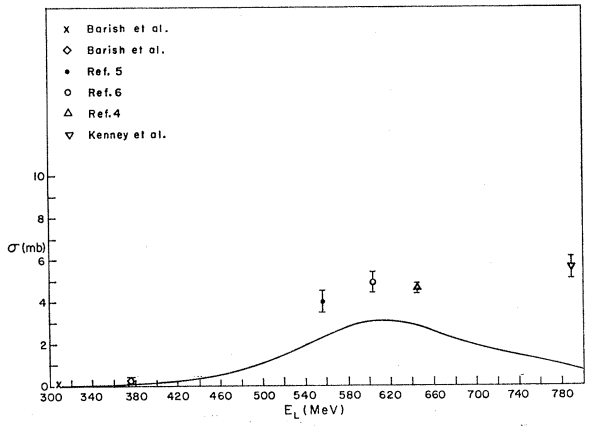

FIG. 4. Cross section generated by the $\rho\Delta\sigma$ model for $\pi^-+p\to\pi^-+\pi^0+p$ from the initial D_{13} state. The references are B. Barish *et al.*, Phys. Rev. **135**, B416 (1964); V. Kenney *et al.*, Bull. Am. Phys. Soc. **8**, 523 (1963).

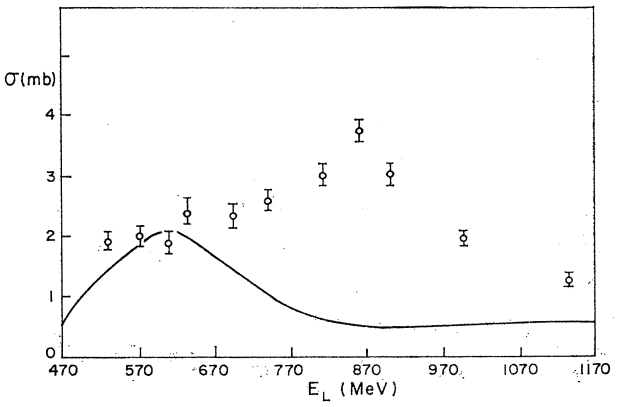

FIG. 5. Cross section generated by the $\rho\Delta\sigma$ model for $\pi^-+p\to\pi^0+\pi^0+n$ from the initial D_{13} state. The experimental points are from C. A. Bordner *et al.*, in *Proceedings of the Twelfth International Conference on High-Energy Physics, Dubna, 1964* (Atomizdat, Moscow, 1966), p. 38.

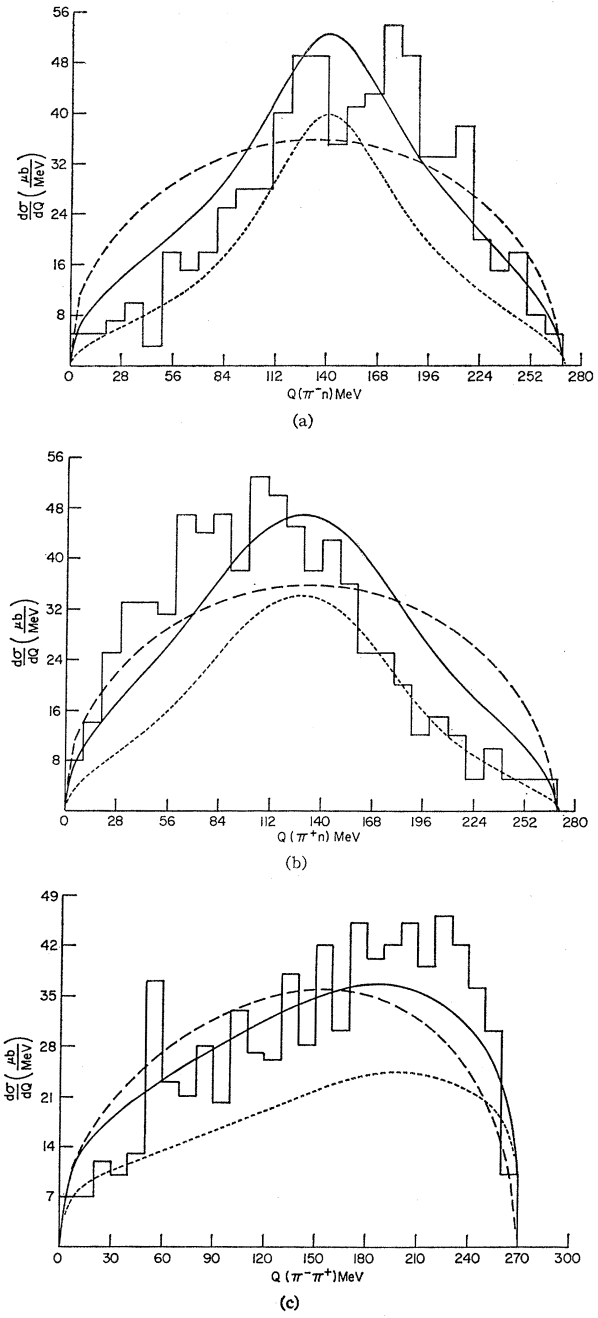

FIG. 6. Parts (a), (b), and (c) contain the $Q(\pi^-n)$, $Q(\pi^+n)$, and $Q(\pi^-\pi^+)$ distributions, respectively, of the $\rho\sigma\Delta$ model at 558 MeV (Ref. 5). Phase space is represented by the dashed curve, while the dotted curve is obtained from the D_{13}-state boundary-condition model. The solid curve illustrates the model curve plus an appropriate amount of phase-space background such that the area under this curve is the experimental cross section. The phase-space background is 36% of the total.

given in Table I. The ρN and σN channels share the strength needed to cause the D_{13} resonance.

The D_{13} phase shift δ_{13} depends chiefly on $\mathrm{Re}f_{\mathrm{eff}}$. It follows that in the resonance region the contribution to $\mathrm{Re}f_{\mathrm{eff}}$ of the ρN and σN channels combined must be approximately the same as the ρN contribution alone in the three-channel model. However, the smaller barrier penetration factor decreases the σ production [Eqs. (25) and (26)] relative to the ρ production for the

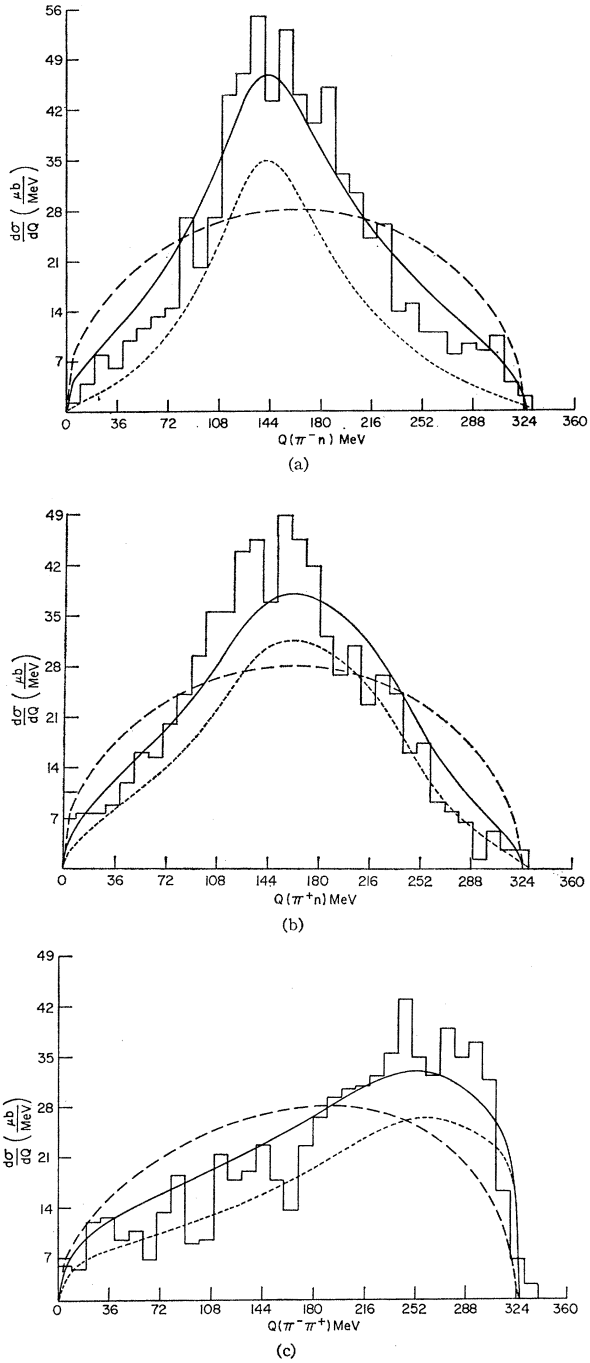

FIG. 7. Parts (a), (b), and (c) contain the $Q(\pi^-n)$, $Q(\pi^+n)$, and $Q(\pi^-\pi^+)$ distributions, respectively, of the $\rho\Delta\sigma$ model at 646 MeV (Ref. 4). The curves are as defined in Fig. 6. The phase-space background is 23% of the total.

same coupling strength. Therefore, to obtain the correct inelasticity parameter η_{13} more Δ coupling is required.

The effect of those changes caused by the addition of the σN channel is to decrease the dipion peaking at the upper end of the mass spectrum in both the $\pi^-\pi^0 p$ and $\pi^+\pi^- n$ final states, because of the smaller total dipion production. The peaking of the $\pi^-\pi^0 p$ final state is very

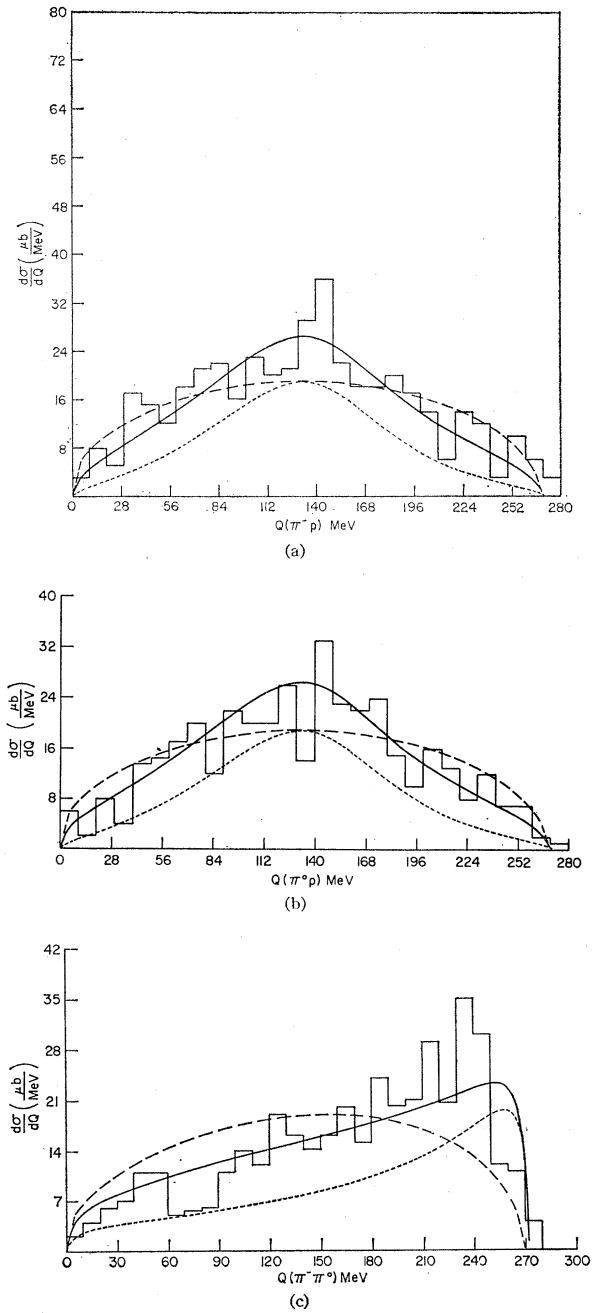

FIG. 8. Parts (a), (b), and (c) contain the $Q(\pi^- p)$, $Q(\pi^0 p)$, and $Q(\pi^-\pi^0)$ distributions, respectively, of the $\rho\Delta\sigma$ model at 558 MeV (Ref. 5). The curves are as defined in Fig. 6. The phase-space background is 40% of the total.

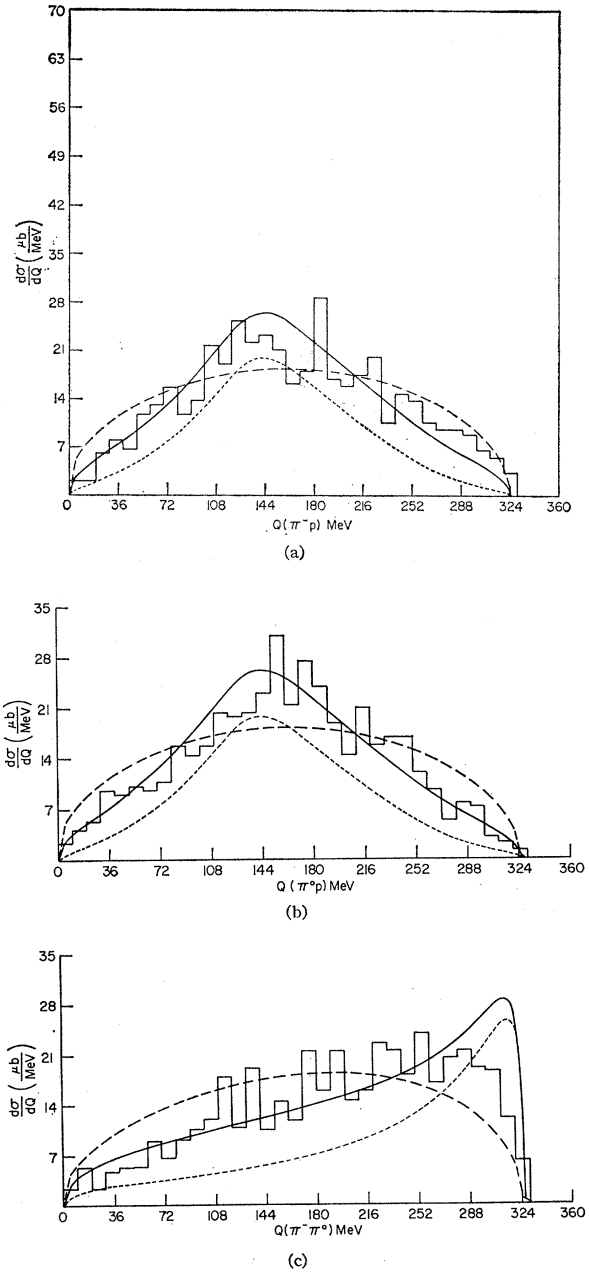

FIG. 9. Parts (a), (b), and (c) contain the $Q(\pi^- p)$, $Q(\pi^0 p)$, and $Q(\pi^-\pi^0)$ distributions, respectively, of the $\rho\Delta\sigma$ model at 646 MeV (Ref. 4). The curves are as defined in Fig. 6. The phase-space background is 50% of the data.

much decreased, as required by the data, because the $T=0$ σ meson does not contribute at all. The dipion peak in the $\pi^+\pi^- n$ final state is also broadened because of the large width of the σ meson. At the same time, the increased proportion of the $\pi\Delta$ final state sharpens the πN barycentric mass peak as required. The D_{13} complex amplitude fit is further improved.

The best fit of the four-channel (πN,$\pi\Delta$,ρN,σN)

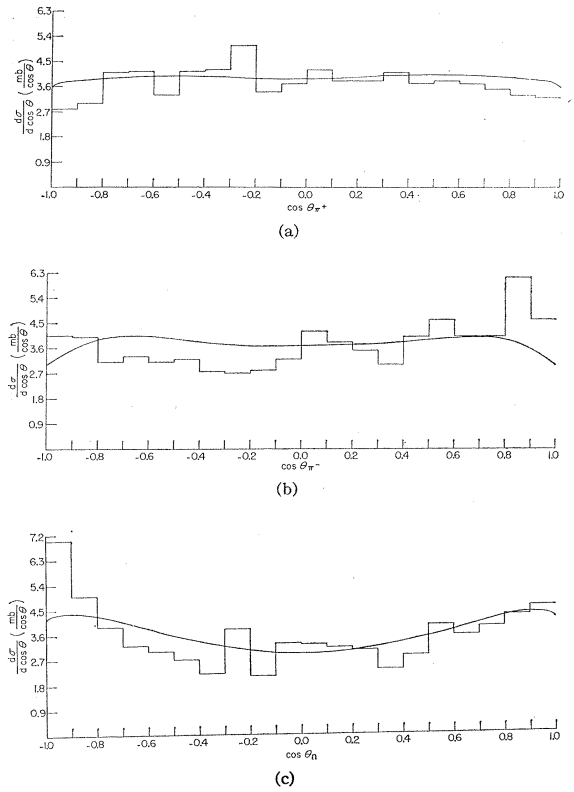

FIG. 10. Parts (a), (b), and (c) show the π^+, π^-, and n angular distributions, respectively, of the reaction $\pi^-+p\rightarrow\pi^-+\pi^++n$ in the over-all COM system at 558 MeV (Ref. 5) from the $\rho\Delta\sigma$ model. The theoretical curve represents the boundary-condition-model D_{13}-state curve plus 36% phase-space background, as indicated in Fig. 6.

system that we have obtained is with

$$f_D=5.55,\quad f_\Delta=2.80,\quad f_\rho=0.40,\quad f_\sigma=0.00,\quad f_{D\Delta}=2.40,\quad f_{D\rho}=2.47,\quad \text{and}\quad f_{D\sigma}=7.00,\tag{60}$$

and a core radius $r_0=0.5\,\mu^{-1}$ as used in all these calculations.[9,10] The results shown in Figs. 2–12 illustrate all the effects of adding the σN channel discussed above. The fit to the complex D_{13} amplitude (Fig. 2) is very good except at energies well below the resonance, where the neglected long-range potential should have an important effect.

Figures 3–5 show the predicted contribution of the D_{13} state to the total $\pi^+\pi^-n$, $\pi^-\pi^0p$, and $\pi^0\pi^0n$ cross sections, σ_T, as a function of energy. In all cases it is seen that from 500 to 700 MeV the D_{13} state accounts for the major part of the cross section. The contribution needed from other states is about 30% in each charge state. Assuming a phase-space form for the background (the proportion is determined by σ_T and is cited in each figure), and incoherent contributions from each channel (as given in Sec. III), the three-body final-state distributions are compared with data in Figs. 6–13. Parts (a) and (b) of Figs. 6–9 show that we obtain a satisfactory πN mass distribution although only 45% of the decays take place through nucleon isobars at 646 MeV and 38% at 558 MeV (this is several times as much nucleon isobar as obtained in the three-channel case[10]). A very marked improvement in the dipion mass distribution is obtained in part (c) of Figs. 6–9, illustrating quantitative agreement. The angular distributions at 558 MeV (Figs. 10 and 12) are quantitatively adequate. At 646 MeV (Figs. 11 and 13), the ratio

$$[\sigma(0°)+\sigma(180°)]/\sigma(90°)$$

agrees satisfactorily with the data, but the model does not predict the observed asymmetry about 90°. This is of course due to the presence of only one partial wave apart from the incoherent phase-space background. At this high end of our energy region, it is reasonable to expect that the D_{15} and F_{15} partial waves are large

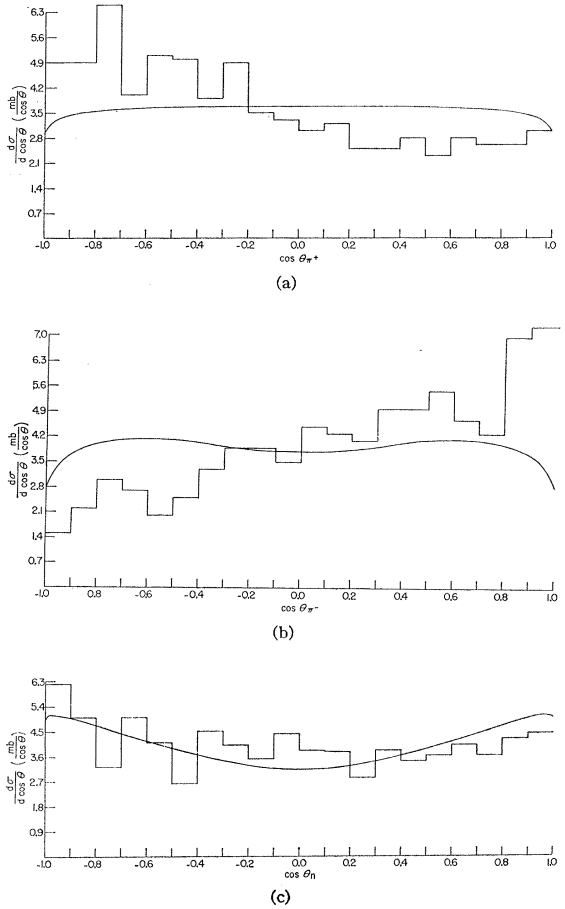

FIG. 11. Parts (a), (b), and (c) show the π^+, π^-, and n angular distributions, respectively, of the reaction $\pi^-+p\rightarrow\pi^-+\pi^++n$ in the over-all COM system at 646 MeV (Ref. 4) from the $\rho\Delta\sigma$ model. The theoretical curve represents the boundary-condition-model D_{13}-state curve plus 23% phase-space background, as indicated in Fig. 7.

enough to show up in angular interference effects, while not necessarily being important apart from such interference effects. For this reason we do not believe that the angular asymmetry at 646 MeV represents an important deficiency of our model. When the D_{15} and F_{15} resonances are treated in a similar way to the present treatment of the D_{13} resonance, the partial-wave interference effects may be predicted.

The ρ, σ, and Δ content of the final state is shown in Fig. 14. At less than 850 MeV (below threshold for the σ and ρ resonance peaks) this content is reflected in the πN and $\pi\pi$ mass distributions in Figs. 6–9. It is also consistent with the proportions deduced approximately from the Dalitz plots,[6,8] which imply that the amounts of dipion and isobar production are approximately equal. At higher energies, e.g., at $E_L=1397$ MeV, our model predicts ρ, σ, and Δ production cross sections to be 0.48, 1.67, and 0.14 mb. Feldman *et al.*[21] determined the $\pi^-+p\rightarrow\sigma+n$ ($\sigma\rightarrow 2\pi^0$ mode) cross section to be 0.18 ± 0.05 mb and the $\pi^-+p\rightarrow\Delta^0\pi^0$ cross section to be 0.27 ± 0.06 mb. Charge symmetry implies that only $\frac{1}{3}$ of the σ mesons produced decay into $2\pi^0$. Similarly, in this experiment only 2/9 of the Δ production is visible. Therefore, assuming charge symmetry, this experiment implies that the total σN cross section is 0.54 mb and the total $\Delta\pi$ cross section is 1.22 mb. Our model for the D_{13} partial wave predicts an inconsistently larger σ production and a consistently smaller Δ production. Data[22] at $E_L=930$ MeV indicate a $\Delta^-\pi^+$ cross section of 6 mb, implying a total Δ production cross section of 12 mb, while the BCM consistently predicts 0.11 mb.

At $E_L=1150$ MeV, Pickup *et al.*[23] find a $\rho^0 n$ cross section of 3.1 mb while the BCM predicts 0.31 mb. Most of the ρ and Δ production may well come from other partial waves, but the cross section of Ref. 21 implies that coupling to higher-mass resonance states

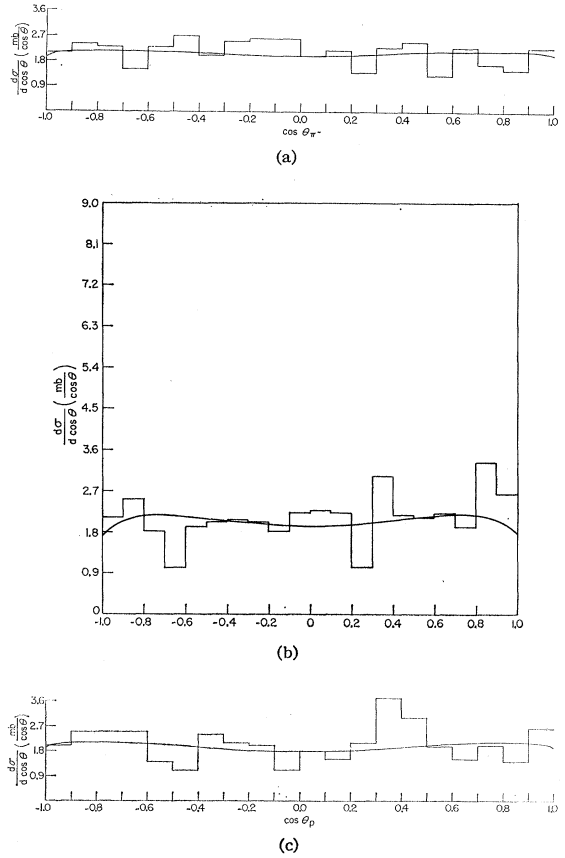

FIG. 12. Parts (a), (b), and (c) show the π^-, π^0, and p angular distributions, respectively, of the reaction $\pi^-+p\rightarrow\pi^-+\pi^0+p$ in the over-all COM system at 558 MeV (Ref. 5). The theoretical curve represents the boundary-condition-model D_{13}-state curve plus 40% phase-space background, as indicated in Fig. 8.

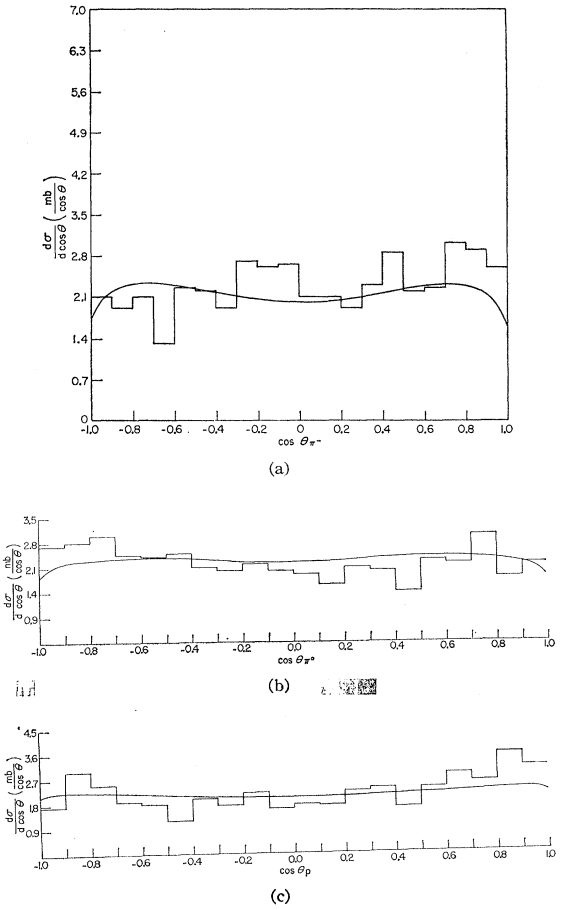

FIG. 13. Parts (a), (b), and (c) show the π^-, π^0, and p angular distributions, respectively, of the reaction $\pi^-+p\rightarrow\pi^-+\pi^0+p$ in the over-all COM system at 646 MeV (Ref. 4). The theoretical curve represents the boundary-condition-model D_{13}-state curve plus 50% phase-space background, as indicated in Fig. 9.

[22] As reported by A. Donnachie, in *Proceedings of the Fourteenth International Conference on High-Energy Physics, Vienna, 1968*, edited by J. Prentki and J. Steinberger (CERN, Geneva, 1968), p. 150.

[23] E. Pickup, D. K. Robinson, and E. O. Salant, Phys. Rev. Letters **9**, 170 (1962); D. R. O. Morrison, Phys. Letters **22**, 528 (1966).

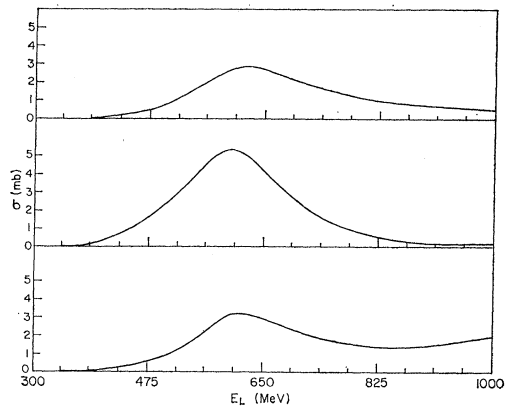

FIG. 14. The (a) ρ, (b) Δ, and (c) σ production cross sections from the initial D_{13} state.

depletes the σN channel at energies above 1 BeV. Candidates are the $D_{15}(1680)$ and $F_{15}(1680)$ paired with a pion, or the ϕ and A resonances paired with a nucleon, or some of the already considered low-mass baryon and meson resonances paired with each other.

The maximum σ width that is consistent with δ and η has been found to be 300 MeV. The δ and η curves with $\Gamma_\sigma > 300$ MeV provide a poor fit to the data because of the large amount of σ meson produced at low energies.

In Figs. 15 and 16, we display our best results for the four-channel (πN,$\pi\Delta$,ρN,ωN) model. There is considerable improvement over the three-channel model, but the dipion spectra are still too sharply peaked. The ω meson does not contribute to the final states; its effect is to decrease the amount of ρ meson and increase the amount of Δ present. The predicted amount of ω production at 1150 MeV is 0.80 mb, consistent with the experimental 1–4 mb for all partial waves.[23]

It is of course likely that the ωN channel is coupled to the system. However, one-pion exchange is prohibited by G parity in the $\pi N \to \omega N$ system, which may well decrease its coupling compared to $\pi N \to \rho N$ and $\pi N \to \sigma N$. It is therefore plausible that the πN, $\pi\Delta$, ρN, and σN channels dominate in our energy range. The addition of some ωN coupling to πN, $\pi\Delta$, ρN, and σN channels would decrease the excessive σ production at high energies. The substantial inelastic threshold cusp shown in Fig. 15 is the result of the S-state stable-particle production. Its experimental observation would confirm this mode of ω-meson production.

Another variation of the channels at our disposal is a three-channel model which contains πN, $\pi\Delta$, and σN. Figure 17 shows the good δ_{13} and η_{13} fits. However, the final-state distributions were unsatisfactory. Figure 18(a) shows the featureless $Q(\pi^-\pi^0)$ distribution resulting from the zero coupling of the σ meson to this channel. Figure 18(b) displays a much too peaked $Q(\pi^- n)$ curve due to an overabundance of Δ (52% compared to 40% in the $\rho\Delta\sigma$ model at the same energy). The good fit to $Q(\pi^-\pi^+)$ in Fig. 18(c) is to be expected in this model but, as demonstrated in Figs. 18(a) and 18(b), a poor fit is obtained for the other distributions.

The final combination, which is a two-channel πN and $\Delta\pi$, has been shown[10] to be incapable of generating the D_{13} resonance (this model corresponds to a Ball-Frazer mechanism).

The calculation of the maximal $\Delta_1\Delta_2$ interference contribution to the $Q_{\pi^-\pi^+}$ distributions, as given in Eq. (59), shows that it has less than a 10% effect (Fig. 19). This is in contrast to the result of Olsson and Yodh,[14] which obtains all the $Q(\pi^-\pi^+)$ peaking from

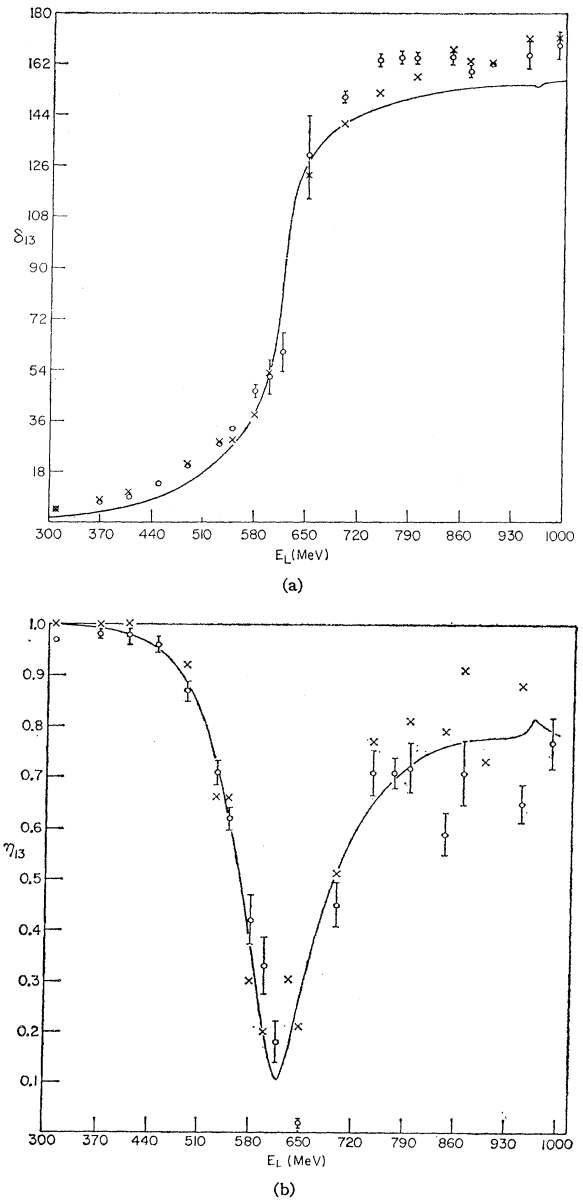

FIG. 15. The $\rho\Delta\omega$ model fit to (a) δ_{13} and (b) η_{13}. The data points are those of Fig. 2. The parameters of the fit are $f_D = 6.42$, $f_\rho = 0.40$, $f_\Delta = 2.80$, $f_\omega = 1.00$, $f_{D\rho} = 7.0$, $f_{D\Delta} = 2.40$, and $f_{D\omega} = 6.20$.

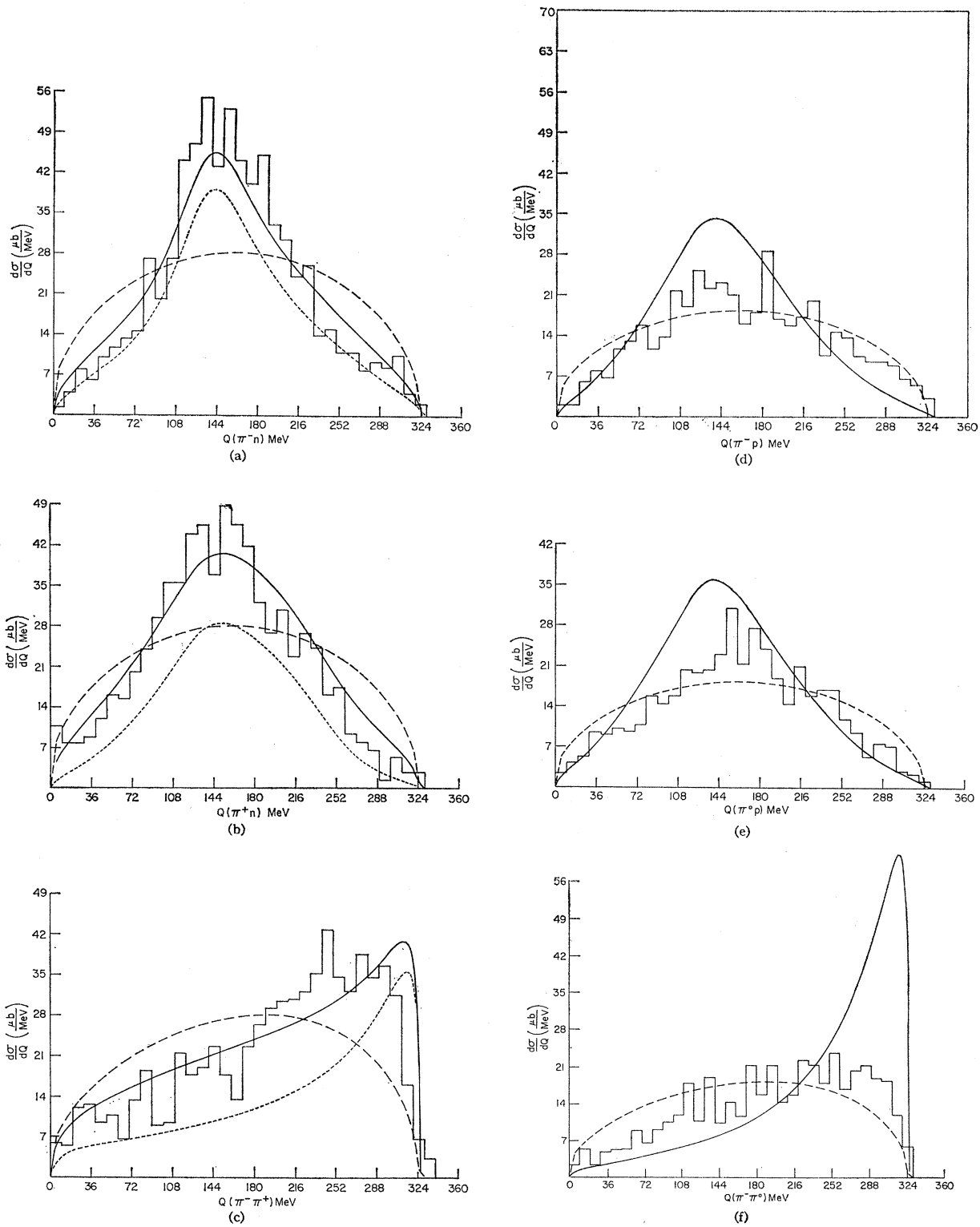

FIG. 16. Parts (a)–(f) represent the final-state Q-value distributions of the $\rho\Delta\omega$ model at 646 MeV (Ref. 4). Graphs (a)–(c) represent the Q-value distributions of the $\pi^-\pi^+n$ final state for which 43% phase-space background was required. These curves are defined in Fig. 6. The distributions from the $\pi^-\pi^0p$ final state [(d)–(f)] have no phase-space background because the production cross section for this reaction is higher than the experimental value. The solid curve represents the boundary-condition-model curve and the dashed curve is phase space.

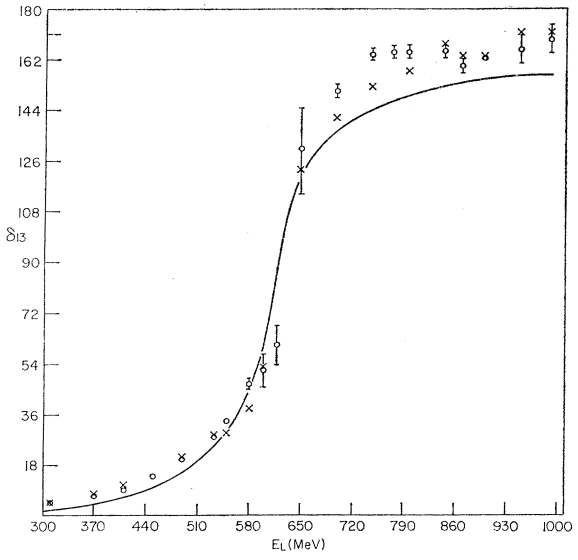

(a)

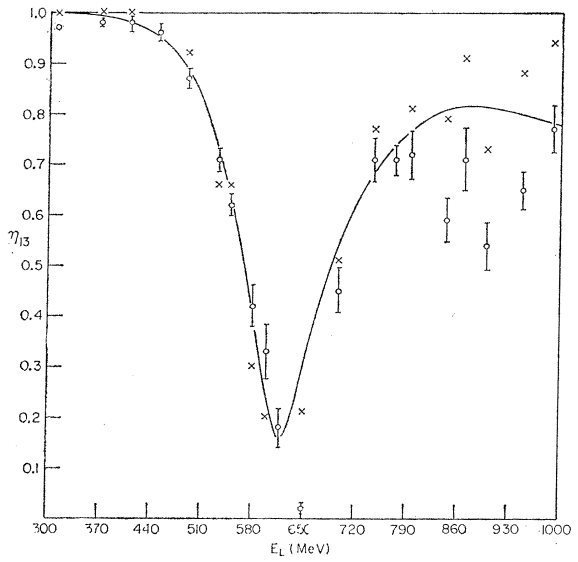

(b)

FIG. 17. $\Delta\sigma$ model fit to (a) δ_{13} and (b) η_{13}. The data points are those of Fig. 2. The parameters of the fit are $f_D=5.52$, $f_\Delta=2.80$, $f_\sigma=0.0$, $f_{D\Delta}=3.00$, and $f_{D\sigma}=9.0$.

their large $\Delta_1\Delta_2$ interference. All other interference terms calculated in this maximal way are small, given the experimental constraints on δ_{13}, η_{13}, and the resonances. The actual interference effects are expected to be even smaller. The data are not accurate enough to discriminate such small effects.

VI. CONCLUSIONS

The good fit to the D_{13} complex amplitude and to the $\pi\pi N$ final-state distributions indicates the adequacy of our model in the region of 400–700-MeV pion kinetic energy. In particular, the D_{13} state accounts for about 70% of the inelastic total cross section, and for all of the structure in the $\pi\pi N$ final states. Furthermore, the four-channel (πN,$\pi\Delta$,ρN,σN) model adequately predicts both the elastic and inelastic amplitudes of the D_{13} state. The amount of coupling required to the $\pi\Delta$ and ρN channels is consistent with resonance production at higher energies. The coupling to the σN channel appears

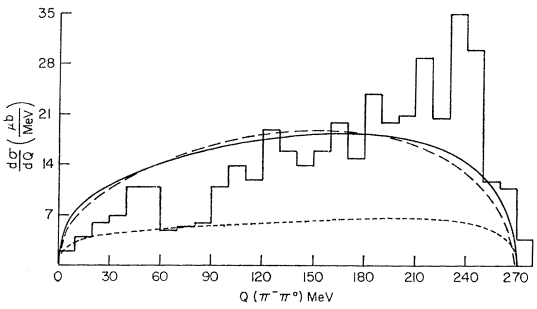

(a)

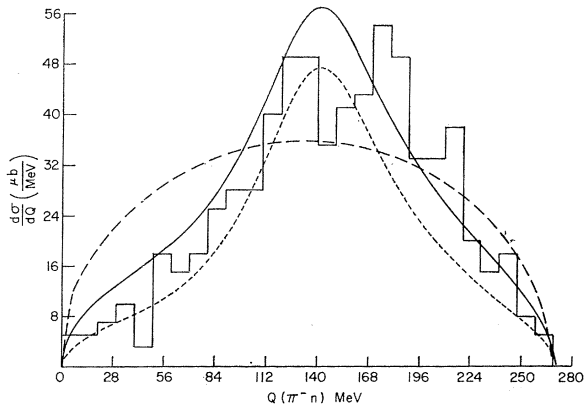

(b)

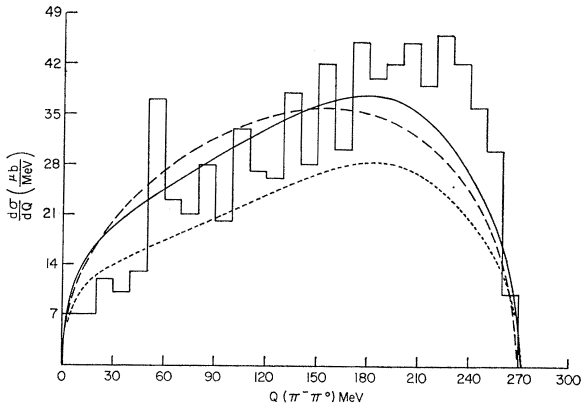

(c)

FIG. 18. Parts (a), (b), and (c) represent the ($\pi^-\pi^0$), (π^-n), and ($\pi^-\pi^+$) Q-value distributions of the $\Delta\sigma$ model at 558 MeV (Ref. 5). The curves are defined in Fig. 6. The $Q(\pi^-\pi^+)$ and $Q(\pi^-n)$ distributions require 28% phase-space background while the $Q(\pi^-\pi^0)$ distribution requires 63% phase-space background.

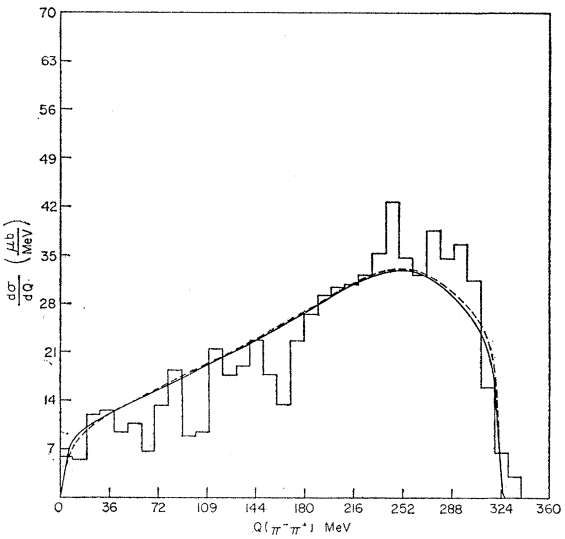

FIG. 19. Maximal $\Delta_1\Delta_2$ interference effect [Eq. (59)] is included in the dashed curve of the $Q_{\pi^+\pi^-}$ distribution at 646 MeV. The solid curve and the data are as in Fig. 7(c).

to need some suppression at higher energies. The dominance of just these channels is also expected on the basis of mass, spin, and the allowed one-pion-exchange mechanism. It has also been demonstrated that even though the four models $(\pi N,\rho N,\Delta\pi)$, $(\pi N,\rho N,\Delta\pi,\sigma N)$, $(\pi N,\rho N,\Delta\pi,\omega N)$, and $(\pi N,\ \Delta\pi,\ \sigma N)$ produced adequate fits to δ and η, the deciding factor between them was the final-state spectra. Only the $(\pi N,\rho N,\ \Delta\pi,\ \sigma N)$ model fitted simultaneously $Q_{\pi\pi}$, $Q_{\pi N}$, δ, and η.

The dynamical coupling model accounts for a significant amount of data for its eight parameters. We feel that its success is due to proper inclusion of unitarity and inelastic threshold dependence, with approximately correct range dependence. A better description of the D_{13} state at low energies would require inclusion of a long-range potential obtained from field theory. This can be done without adding parameters to the model. At higher energies, it would become necessary to include the coupling to other channels. Interference effects between decaying resonances should be calculated with the spatial decay distribution taken into account, but are of little importance.

Refinement of the description of inelastic final states will also require that other partial waves be analyzed to a similar extent as the D_{13}. This appears to be a feasible program for the resonant P_{11}, D_{15}, and F_{15} amplitudes. Together with the D_{13} amplitude these are likely to dominate the $T=\frac{1}{2}$ πN amplitude up to 1 BeV.

ACKNOWLEDGMENTS

The valuable assistance of Mrs. Nancy Spencer with the programming and the services of the Laboratory of Nuclear Science Computer Facility are gratefully acknowledged. One of us (A. I. M.) thanks Professor H. Feshbach for the hospitality extended to him at the Center for Theoretical Physics at the Massachusetts Institute of Technology. He also thanks the Laboratory of Nuclear Science at MIT for the use of its facilities.

APPENDIX A

In this appendix we shall indicate some relevant kinematical relationships. The numerical calculations leading to our results are carried out in the over-all COM system, where $\mathbf{q}_1+\mathbf{q}_2+\mathbf{P}=0$.

The resonance masses are defined as

$$M_{\Delta_1}{}^2=-(P+q_1)^2, \tag{A1}$$

$$M_{\Delta_2}{}^2=-(P+q_2)^2, \tag{A2}$$

$$M_{\rho,\sigma}{}^2=-(q_1+q_2)^2 \tag{A3}$$

(where P_1, q_1, and q_2 are four-vectors), and are related by the constraint equation

$$M_{\Delta_1}{}^2+M_{\Delta_2}{}^2+M_{\rho,\sigma}{}^2=2\mu^2+M^2+W^2. \tag{A4}$$

Evaluating (A1)–(A3) in the over-all COM system, we have

$$M_{\Delta_1}=(W^2+\mu^2-2W\omega_2)^{1/2}, \tag{A5}$$

$$M_{\Delta_2}=(W^2+\mu^2-2W\omega_1)^{1/2}, \tag{A6}$$

$$M_{\rho,\sigma}=(W^2+M^2-2WE)^{1/2}, \tag{A7}$$

where ω_i and E are, respectively, the energies of the ith pion and of the nucleon in the over-all COM system. Evaluating (A1)–(A3) in the respective resonance COM system, we have

$$M_{\Delta_1}=(q_1{}^{(1)2}+M^2)^{1/2}+(q_1{}^{(1)2}+\mu^2)^{1/2}, \tag{A8}$$

$$M_{\Delta_2}=(q_2{}^{(2)2}+M^2)^{1/2}+(q_2{}^{(2)2}+\mu^2)^{1/2}, \tag{A9}$$

$$M_{\rho,\sigma}=2(q_1{}^{(3)2}+\mu^2)^{1/2}. \tag{A10}$$

From energy-momentum conservation, we can derive the following equations when $i,\ j=1,\ 2$ or $2,\ 1$:

$$q_i=\frac{-\frac{1}{2}(M_{\Delta_i}{}^2-M^2+\mu^2)q_j\cos\theta_{12}\pm(W+\omega_j)[q_i{}^{(1)2}M_{\Delta_i}{}^2-q_j{}^2(1-\cos^2\theta_{12})\mu^2]^{1/2}}{M_{\Delta_i}{}^2+q_j{}^2(1-\cos^2\theta_{12})}, \tag{A11}$$

$$q_2=\frac{-\frac{1}{2}M_3{}^2P\cos\theta_{2N}\pm(W-E)[M_3{}^2q_2{}^{(3)2}-P^2(1-\cos^2\theta_{2N})\mu^2]^{1/2}}{M_3{}^2+P^2(1-\cos^2\theta_{2N})}, \tag{A12}$$

$$P=\frac{-\frac{1}{2}[M_{\Delta_i}{}^2+M^2-\mu^2]q_j\cos\theta_{jN}\pm(W-\omega_j)[M_{\Delta_i}{}^2P^{(1)2}-M^2q_j{}^2(1-\cos^2\theta_{jN})]^{1/2}}{M_{\Delta_i}{}^2+q_j{}^2(1-\cos^2\theta_{jN})}. \tag{A13}$$

The integration limits for the Q value and angular distributions are quite complicated owing to the three-body kinematics. However, the procedure for determining the integration limits is straightforward but lengthy, so we shall only indicate how the Δ_1 Q-value term is done.

The term to be evaluated is [see Eq. (42)]

$$\frac{d\sigma}{dM_{\Delta_1}} = \int_{-1}^{g(M_{\Delta_1})} d\cos\theta_{12}\, f(M_{\Delta_i},\cos\theta_{12}) \quad \text{(A14)}$$

(where $dM_{\Delta_1}=dQ_{\Delta_1}$). The maximum and minimum values of M_{Δ_1}, i.e., $W-\mu>M_{\Delta_1}>M+\mu$, determine the minimum and maximum values of q_2.

Solving Eq. (A5) for q_2, we have

$$q_2=\{[W^2-(M_{\Delta_1}+\mu)^2]\times[W^2-(M_{\Delta_1}-\mu)^2]\}^{1/2}/2W. \quad \text{(A15)}$$

Therefore, when $M_{\Delta_1}=(M_{\Delta_1})_{\max}=W-\mu$ we have $q_2=0$, and when $M_{\Delta_1}=(M_{\Delta_1})_{\min}=M+\mu$ we have

$$q_2=q_{2\max}=\{[(W+M+\mu)^2-\mu^2]\times[(W-(M+\mu)]^2-\mu^2]\}^{1/2}/2W. \quad \text{(A16)}$$

We must now find the dependence of cos θ_{12} on q_2. In Eq. (A11) set $i=1$ and $j=2$:

$$q_1=\frac{-\frac{1}{2}[M_{\Delta_1}{}^2-M^2+\mu^2]q_2\cos\theta_{12}\pm(W-\omega_2)[q_1{}^{(1)2}M_{\Delta_1}{}^2-q_2{}^2(1-\cos^2\theta_{12})\mu^2]^{1/2}}{M_{\Delta_1}{}^2-q_2{}^2(1-\cos^2\theta_{12})}. \quad \text{(A17)}$$

For values of q_2 between zero and the value where $q_1=0$, it is possible for π_1 to have any orientation with respect to π_2 [the positive sign in (A17) in front of the square root is used in this range]. The value of q_2 for which $q_1=0$ we call q_{2c}, which is

$$q_{2c}=\{[(W-\mu)^2-(M+\mu)^2]\times[(W-\mu)^2-(M-\mu)^2]\}^{1/2}/2(W-\mu). \quad \text{(A18)}$$

For $q_2>q_{2c}$ the velocity of π_1 in the Δ_1 rest frame is less than the velocity of Δ_1 relative to the over-all COM frame. We then have the possibility that the argument of the radical in (A17) can become negative, giving an imaginary q_1.

Therefore, when $q_2>q_{2c}$ we set the discriminant in (A13) to zero and solve for cosθ_{12} as a function of q_2 (and therefore of M_{Δ_1}):

$$g(M_{\Delta_1})=-[\mu^2q_2{}^2-q_1{}^{(1)2}M_{\Delta_1}{}^2]^{1/2}/\mu q_2. \quad \text{(A19)}$$

The negative root is chosen in (A19) because when $q_2>q_{2c}$ the first term in the numerator of (A17) is bigger than the second term. Since $q_1>0$ we must have $\cos\theta_{12}<0$. The integration limits are

$0\leq q_2\leq q_{2c}$, $g(M_{\Delta l_1})=1$, [+sign only in front of square root in (A17)];

$q_{2c}<q_2\leq q_{2\max}$, $g(M_{\Delta_1})=-[\mu^2q_2{}^2-q_1{}^{(1)2}M_{\Delta_1}{}^2]/\mu q_2$, [±sign in (A17)].

APPENDIX B

The following transformations are used to derive the Lorentz transformation Jacobians when $(i,j)=(1,2)$ or $(2,1)$:

$$\mathbf{q}_i{}^{(i)}=\mathbf{q}_i+\mathbf{X}_i{}^j\mathbf{q}_j, \quad \text{(B1)}$$

$$\mathbf{q}_i{}^{(3)}=\mathbf{q}_i+\mathbf{X}_i{}^3\mathbf{P}, \quad \text{(B2)}$$

$$\mathbf{P}^{(i)}=\mathbf{P}+\mathbf{X}_N{}^j\mathbf{q}_j, \quad \text{(B3)}$$

where

$$\mathbf{X}_i{}^j=\frac{\omega_i+\omega_i{}^{(i)}}{W-\omega_j+M_{\Delta_i}}, \quad \mathbf{X}_N{}^j=\frac{E+E^{(i)}}{W-\omega_j+M_{\Delta_i}}, \quad \text{(B4)}$$

$$\mathbf{X}_i{}^3=(\omega_i+\omega_i{}^{(3)})/(W-E+M_3) \quad \text{(B5)}$$

[the superscript (i) indicating the appropriate COM resonance].

We shall present in detail the derivation of $J(\mathbf{q}_2{}^{(3)}|\mathbf{q}_2)$. The procedures for the other Jacobians are exactly analogous.

The quantity $J(\mathbf{q}_2{}^{(3)}|\mathbf{q}_2)$ which transforms π_2 from the rest system to the over-all c.m. system is defined as

$$J(\mathbf{q}_2{}^{(3)}|\mathbf{q}_2)=\left(\frac{\partial q_2{}^{(3)}}{\partial q_2}\right)_{\theta_{2N}}\left(\frac{\partial\cos\theta_{2N}{}^{(3)}}{\partial\cos\theta_{2N}}\right)_{q_2}-\left(\frac{\partial q_2{}^{(3)}}{\partial\cos\theta_{2N}}\right)_{q_2}\left(\frac{\partial\cos\theta_{2N}{}^{(3)}}{\partial q_2}\right)_{\theta_{2N}}. \quad \text{(B6)}$$

The Lorentz-transformation direction is along the recoil nucleon; therefore

$$\mathbf{P}=W^{-1}M_3\mathbf{P}^{(3)}, \quad \text{(B7)}$$

which also implies that

$$d\Omega_N=d\Omega_N{}^{(3)}. \quad \text{(B8)}$$

[A similar situation pertains to Eq. (38).]

From (B2), we have

$$(q_2{}^{(3)})^2=q_2{}^2+(X_2{}^3)^2P^2+2q_2PX_2{}^3\cos\theta_{2N}, \quad \text{(B9)}$$

$$\cos\theta_{2N}{}^{(3)}=(q_2\cos\theta_{2N}+X_2{}^3P)/q_2{}^{(3)}. \quad \text{(B10)}$$

The derivatives in (B6) can now be obtained from

(B9) and (B10):

$$\left(\frac{\partial q_2^{(3)}}{\partial q_2}\right)_{\theta_{2N}}=\frac{1}{q_2^{(3)}}\left[(q_2+PX_2{}^3\cos\theta_{2N})+(PX_2{}^3+q_2\cos\theta_{2N})\left(\frac{\partial(X_2{}^3P)}{\partial q_2}\right)_{\theta_{2N}}\right], \tag{B11}$$

$$\left(\frac{\partial q_2{}^{(3)}}{\partial\cos\theta_{2N}}\right)_{q_2}=\frac{1}{q_2{}^{(3)}}\left[q_2PX_2{}^3+(PX_2{}^3+q_2\cos\theta_{2N})\left(\frac{\partial(X_2{}^3P)}{\partial\cos\theta_{2N}}\right)_{q_2}\right], \tag{B12}$$

$$\left(\frac{\partial\cos\theta_{2N}{}^{(3)}}{\partial\cos\theta_{2N}}\right)_{q_2}=\frac{1}{q_2{}^{(3)}}\left[q_2+\left(\frac{\partial(X_2{}^3P)}{\partial\cos\theta_{2N}}\right)_{q_2}-\cos\theta_{2N}{}^{(3)}\left(\frac{\partial q_2{}^{(3)}}{\partial\cos\theta_{2N}}\right)_{q_2}\right], \tag{B13}$$

$$\left(\frac{\partial\cos\theta_{2N}{}^{(3)}}{\partial q_2}\right)_{\theta_{2N}}=\frac{1}{q_2{}^{(3)}}\left[q_2+\left(\frac{\partial(X_2{}^3P)}{\partial q_2}\right)_{\theta_{2N}}-\cos\theta_{2N}{}^{(3)}\left(\frac{\partial q_2{}^{(3)}}{\partial q_2}\right)_{\theta_{2N}}\right]. \tag{B14}$$

Substituting (B11)–(B14) into (B6), we obtain

$$J(\mathbf{q}_2{}^{(3)}|\mathbf{q}_2)=\left(\frac{q_2}{q_2{}^{(3)}}\right)^2\left[1+\frac{\sin^2\theta_{2N}}{q_2}\left(\frac{\partial(\mathbf{X}_2{}^3P)}{\partial\cos\theta_{2N}}\right)_{q_2}+\cos\theta_{2N}\left(\frac{\partial(\mathbf{X}_2{}^3P)}{\partial q_2}\right)_{\theta_{2N}}\right], \tag{B15}$$

where

$$\left(\frac{\partial(\mathbf{X}_2{}^3P)}{\partial q_2}\right)_{\theta_{2N}}=q_2P\omega_2{}^{-1}(W-E+M_3)^{-1}+\left(\frac{\partial P}{\partial q_2}\right)_{\theta_{2N}}\times\left\{\left[\mathbf{X}_2{}^3\left(1+\frac{W}{M_3}\right)-\frac{W}{2M_3}\right]\times\frac{P^2}{E(W-E+M_3)}+\mathbf{X}_2{}^3\right\}, \tag{B16}$$

$$\left(\frac{\partial(\mathbf{X}_2{}^3P)}{\partial\cos\theta_{2N}}\right)_{q_2}=\left(\frac{\partial P}{\partial\cos\theta_{2N}}\right)_{q_2}\left\{\left[\mathbf{X}_2{}^3\left(1+\frac{W}{M_3}\right)-\frac{W}{2M_3}\right]\times\frac{P^2}{E(W-E+M_3)}+\mathbf{X}_2{}^3\right\}. \tag{B17}$$

The derivatives are evaluated from (A13) with $i=1$ and $j=2$.

The other relevant Jacobians are with i, $j=1$, 2,

$$J(\mathbf{q}_i{}^{(i)}|\mathbf{q}_i)=\left(\frac{q_i}{q_i{}^{(i)}}\right)^2\left[1+\frac{\sin^2\theta_{ij}}{q_i}\left(\frac{\partial(\mathbf{X}_i{}^jq_j)}{\partial\cos\theta_{ij}}\right)_{q_i}+\cos\theta_{ij}\left(\frac{\partial(\mathbf{X}_i{}^jq_j)}{\partial q_i}\right)_{\theta_{ij}}\right], \tag{B18}$$

$$J(\mathbf{P}^{(i)}|\mathbf{P})=\left(\frac{P}{P^{(i)}}\right)^2\left[1+\frac{\sin^2\theta_{jN}}{P}\left(\frac{\partial(\mathbf{X}_N{}^jq_j)}{\partial\cos\theta_{jN}}\right)_P+\cos\theta_{jN}\left(\frac{\partial(\mathbf{X}_N{}^jq_j)}{\partial P}\right)_{\theta_{jN}}\right], \tag{B19}$$

where all derivatives are evaluated using (A11)–(A13).

APPENDIX C

Reduction to Relative Angle

In Secs. III and IV of this paper we consider integrals of the form

$$\int_0^{2\pi}\int_{-1}^{1}\int_0^{2\pi}\int_{-1}^{1}d\cos\theta_A\,d\phi_A d\cos\theta_B\,d\phi_B\,f(\theta_{AB})\times[\hat{t}_A\cdot\hat{t}_B+3(\hat{t}_A\cdot\hat{z})(\hat{t}_B\cdot\hat{z})], \tag{C1}$$

in which θ_A, ϕ_A, θ_B, and ϕ_B are the polar and azimuthal angles of two vectors $\mathbf{q}_A$ and $\mathbf{q}_B$ in the over-all COM system, and θ_{AB} is the angle between $\mathbf{q}_A$ and $\mathbf{q}_B$. The unit vector $\hat{t}_A$ ($\hat{t}_B$) is either in the direction of $\mathbf{q}_A$ ($\mathbf{q}_B$) or in the direction of $\mathbf{q}_A{}^B$ ($\mathbf{q}_B{}^A$), the Lorentz transformation of $\mathbf{q}_A$ ($\mathbf{q}_B$) by the velocity corresponding to $-\mathbf{q}_B$ ($-\mathbf{q}_A$). The above Lorentz transformation translates to the COM system of the resonance paired with the particle of momentum $\mathbf{q}_B$ ($\mathbf{q}_A$). Fortunately, all these four-dimensional integrals can be reduced to an integral over θ_{AB} alone.

In proving the above assertion, we obtain first (i) the Jacobian of transformation of the variable ϕ_B to $\cos\theta_{AB}$. Then we establish (ii) that $\hat{t}_A\cdot\hat{t}_B$ depends only on θ_{AB} and find the expression for $3(\hat{t}_A\cdot\hat{z})(\hat{t}_B\cdot\hat{z})$ as a function of θ_A, θ_B, and θ_{AB}. Finally (iii) the integrations on $\cos\theta_A$, $\cos\theta_B$, and ϕ_A are performed, and it is shown that the integral of $3(\hat{t}_A\cdot\hat{z})(\hat{t}_B\cdot\hat{z})$ is equal to the integral of $\hat{t}_A\cdot\hat{t}_B$. Consequently the integral (C1) is proportional to the integral of $f(\theta_{AB})\hat{t}_A\cdot\hat{t}_B$ with respect to $\cos\theta_{AB}$.

(i) The angular transformation is conveniently performed in two steps,

$$\phi_B\rightarrow\phi_{AB}\equiv\phi_B-\phi_A \tag{C2}$$

and

$$\phi_{BA}\rightarrow\cos\theta_{AB}. \tag{C3}$$

The Jacobian of (C2) is trivially unity, and the range of integration in ϕ_{AB} remains $0\rightarrow2\pi$. The transformation (C3) is given by

$$\cos\theta_{AB}=\cos\theta_A\cos\theta_B+\sin\theta_A\sin\theta_B\cos\phi_{AB}, \tag{C4}$$

from which one derives

$$J(\phi_{AB}|\cos\theta_{AB}) = \left|\left(\frac{\partial\phi_{AB}}{\partial\cos\theta_{AB}}\right)_{\theta_A,\theta_B}\right| = |(\sin\phi_{AB}\sin\theta_A\sin\theta_B)^{-1}|$$
$$= [1-\cos^2\theta_A-\cos^2\theta_B-\cos^2\theta_{AB} +2\cos\theta_A\cos\theta_B\cos\theta_{AB}]^{-1/2}. \quad \text{(C5)}$$

The transformation also implies changes in the boundaries of integration. As ϕ_{AB} spans $0\to 2\pi$, θ_{AB} spans $|\theta_A-\theta_B|$ to $\theta_A+\theta_B$ twice. This implies that if θ_A and θ_B are held fixed,

$$\int_0^{2\pi} d\phi_{BA} \to 2\int_{\cos(\theta_A+\theta_B)}^{\cos(\theta_A-\theta_B)} J(\phi_{AB}|\cos\theta_{AB})\,d\cos\theta_{AB}. \quad \text{(C6)}$$

Below we actually perform integrations over θ_A and θ_B first, and limits are appropriately interchanged.

(ii) We treat the cases $\hat{t}_A=\mathbf{q}_A{}^B/q_A{}^B$ and $\hat{t}_B=\mathbf{q}_B{}^A/q_B{}^A$. The other cases are obtained by an analogous but simpler procedure. The Lorentz transformation for $\mathbf{q}_A$ is

$$\mathbf{q}_A{}^B=\mathbf{q}_A+\mathbf{X}_A{}^B\mathbf{q}_B,$$

with

$$\mathbf{X}_A{}^B=(E_A+E_A{}^B)(W-E_A+E_B{}^B+E_C{}^B)^{-1}, \quad \text{(C7)}$$

in which E_A, E_B, $E_A{}^B$, and $E_B{}^A$ are the energies of the particles with momentum $\mathbf{q}_A$ and $\mathbf{q}_B$ in the over-all COM system and the resonance COM system, respectively. $\mathbf{q}_B{}^A$ is given by an analogous formula to (C7).

The important property of $\mathbf{X}_A{}^B$ and $\mathbf{X}_B{}^A$ is that they depend only on θ_{AB}; the above energies depend only on the particle masses, W, and θ_{AB}, as detailed in Appendix A. From (C7) it also follows immediately that $g_A{}^B$ depends only θ_{AB}, as does $q_B{}^A$.

From (C7) one obtains

$$\hat{q}_A{}^B\cdot\hat{q}_B{}^A=(q_A{}^Bq_B{}^A)^{-1}[q_Aq_B(1+\mathbf{X}_A{}^B\mathbf{X}_B{}^A)\cos\theta_{AB} +\mathbf{X}_A{}^Bq_B{}^2+\mathbf{X}_B{}^Aq_A{}^2], \quad \text{(C8)}$$

which depends only on θ_{AB}. It also follows that

$$(\hat{q}_A{}^B\cdot\hat{z})(\hat{q}_B{}^A\cdot\hat{z})=(q_A{}^Bq_B{}^A)^{-1} \times[q_Aq_B(1+\mathbf{X}_A{}^B\mathbf{X}_B{}^A)\cos\theta_A\cos\theta_B +\mathbf{X}_A{}^Bq_B{}^2\cos^2\theta_B+\mathbf{X}_B{}^Aq_A{}^2\cos^2\theta_A]. \quad \text{(C9)}$$

The expressions for $\hat{q}_A\cdot\hat{q}_B{}^A$ and $(\hat{q}_A\cdot\hat{z})(\hat{q}_B{}^A\cdot\hat{z})$ are obtained from the above by replacing $\mathbf{X}_A{}^B$ with zero, and $q_A{}^B$ with q_A, and so on for the other $\hat{t}_A$ and $\hat{t}_B$ combinations.

(iii) We first integrate

$$J_1=\int_0^{2\pi}\int_{-1}^{1}\int_0^{2\pi}\int_{-1}^{1} d\cos\theta_A d\phi_A d\cos\theta_B\,d\phi_B\,f(\theta_{AB})\hat{q}_A{}^B\cdot\hat{q}_B{}^A$$
$$=2\int_{-1}^{1} d\cos\theta_{AB}\,f(\theta_{AB})\hat{q}_A{}^B\cdot\hat{q}_B{}^A\int_0^{2\pi}d\phi_A\int_{-1}^{1}d\cos\theta_A\int_{\cos(\theta_{AB}+\theta_A)}^{\cos(\theta_{AB}-\theta_A)} d\cos\theta_B\,J(\phi_{AB}|\cos\theta_{AB})$$
$$=4\pi\int_{-1}^{1} d\cos\theta_{AB}\,f(\theta_{AB})\hat{q}_A{}^B\cdot\hat{q}_B{}^A\int_{-1}^{1}d\cos\theta_A\int_{\cos(\theta_{AB}+\theta_A)}^{\cos(\theta_{AB}-\theta_A)} d\cos\theta_B$$
$$\times(1-\cos^2\theta_A-\cos^2\theta_B-\cos^2\theta_{AB}+2\cos\theta_A\cos\theta_B\cos\theta_{AB})^{-1/2}$$
$$=4\pi\int_{-1}^{1} d\cos\theta_{AB}\,f(\theta_{AB})\hat{q}_A{}^B\cdot\hat{q}_B{}^A\int_{-1}^{1}d\cos\theta_A\sin^{-1}\left(\frac{y-\cos\theta_A\cos\theta_{AB}}{\sin\theta_{AB}\sin\theta_A}\right)_{y=\cos(\theta_{AB}+\theta_A)}^{y=\cos(\theta_{AB}-\theta_A)}$$
$$=4\pi^2\int_{-1}^{1} d\cos\theta_{AB}\,f(\theta_{AB})\hat{q}_A{}^B\cdot\hat{q}_B{}^A\int_{-1}^{1}d\cos\theta_A$$
$$=8\pi^2\int_{-1}^{1} d\cos\theta_{AB}\,f(\theta_{AB})\hat{q}_A{}^B\cdot\hat{q}_B{}^A. \quad \text{(C10)}$$

Next we integrate [skipping steps similar to those in (C10)]

$$J_2=3\int_0^{2\pi}\int_{-1}^{1}\int_0^{2\pi}\int_{-1}^{1} d\cos\theta_A\, d\phi_A d\cos\theta_B\, d\theta_B\, f(\theta_{AB})(\hat{q}_A{}^B\cdot\hat{z})(\hat{q}_B{}^A\cdot\hat{z})$$

$$=12\pi\int_{-1}^{1} d\cos\theta_{AB}\frac{f(\theta_{AB})}{q_A{}^B q_B{}^A}\Bigg\{\int_{-1}^{1} d\cos\theta_A\int_{\cos(\theta_{AB}+\theta_A)}^{\cos(\theta_{AB}-\theta_A)} d\cos\theta_B\, J(\phi_{AB}|\cos\theta_{AB})$$

$$\times[q_A q_B(1+\mathbf{X}_A{}^B\mathbf{X}_B{}^A)\cos\theta_A\cos\theta_B+\mathbf{X}_B{}^A q_A{}^2\cos^2\theta_A]$$

$$+\int_{-1}^{1} d\cos\theta_B\int_{\cos(\theta_{AB}+\theta_A)}^{\cos(\theta_{AB}-\theta_A)} d\cos\theta_A\, J(\phi_{AB}|\cos\theta_{AB})\mathbf{X}_A{}^B q_B{}^2\cos^2\theta_B\Bigg\}$$

$$=8\pi^2\int_{-1}^{1} d\cos\theta_{AB}\frac{f(\theta_{AB})}{q_A{}^B q_B{}^A}[q_A q_B(1+\mathbf{X}_A{}^B\mathbf{X}_B{}^A)\cos\theta_{AB}+\mathbf{X}_B{}^A q_A{}^2+\mathbf{X}_A{}^B q_B{}^2]$$

$$=8\pi^2\int_{-1}^{1} d\cos\theta_{AB}\, f(\theta_{AB})\hat{q}_A{}^B\cdot\hat{q}_B{}^A=J_1. \tag{C11}$$

Similarly, one obtains $J_1=J_2$ when $\hat{t}_A$ or $\hat{t}_B$ is $\hat{q}_A$ or $\hat{q}_B$ instead of $\hat{q}_A{}^B$ or $q_B{}^A$. The integral in (C1) is twice the integral J_1, and only the integral over $\cos\theta_{AB}$ remains to be performed numerically.

PHYSICAL REVIEW D VOLUME 2, NUMBER 7 1 OCTOBER 1970

Some Comments on Baryonic States

R. P. FEYNMAN
California Institute of Technology, Pasadena, California 91109

AND

S. PAKVASA* AND S. F. TUAN*
University of Hawaii, Honolulu, Hawaii 96822

(Received 15 June 1970)

We discuss some regularities in the baryon mass spectrum which have been suggested by one of us and possible experimental verification of them.

IN this paper we should like to call attention to certain approximate regularities among the square masses of the baryons with the hope that future research can establish whether they are real or are the result of numerical accidents in the limited data available.

Our classification of states will be guided by the three-quark model of "baryons" and the principle of Regge recurrence. The states[1] of three quarks each of spin $\frac{1}{2}$ depend on the symmetry character of the state. If it is symmetric, it is a **56** (consisting of a spin-quartet unitary-spin decimet, ^{4}10, and a spin-doublet unitary-spin octet, ^{2}8). If it is antisymmetric it is a **20** (spin-doublet unitary-spin octet, ^{2}8, and a spin-quartet singlet, ^{4}1). For the intermediate symmetry, we have the double representation of a **70**$=^2$1, ^{2}8, ^{4}8, ^{2}10.

We next suppose that the over-all state is entirely symmetric. If we add internal degrees of freedom, we suppose that the lowest states are the s states, themselves symmetric and of zero angular momentum. Thus our lowest states are

$$(\mathbf{56},0^+)=^2 8_{1/2}{}^+,\ ^4 10_{3/2}{}^+,$$

where the ${}^a b_j{}^p$ give spin multiplicity a, unitary spin multiplicity b, parity p, and angular momentum j of the states. These, of course, are taken to be the fundamental octet and the lowest decimet (with $\Delta=1236$).

We may expect this to recur on a Regge trajectory[2] by adding 2, 4, ... units of angular momentum (which

* Work supported in part by the U. S. Atomic Energy Commission.

[1] O. W. Greenberg, Phys. Rev. Letters **13**, 598 (1964).

[2] G. F. Chew and S. C. Frautschi, Phys. Rev. Letters **7**, 394 (1961); **8**, 41 (1962).